Article

SOURCE DATA | TRANSPARENT PROCESS

EMBO reports

CK1-mediated phosphorylation of FAM110A promotes its interaction with mitotic spindle and controls chromosomal alignment

Cecilia Aquino Perez, Monika Burocziova, Gabriela Jenikova & Libor Macurek*

Abstract

Progression through the cell cycle is driven by cyclin-dependent kinases that control gene expression, orchestration of mitotic spindle, and cell division. To identify new regulators of the cell cycle, we performed transcriptomic analysis of human non-transformed cells expressing a fluorescent ubiquitination-based cell cycle indicator and identified 701 transcripts differentially expressed in G1 and G2 cells. Family with sequence similarity 110 member A (FAM110A) protein is highly expressed in G2 cells and localized at mitotic spindle and spindle poles during mitosis. Depletion of FAM110A impairs chromosomal alignment, delays metaphase-to-anaphase transition, and affects spindle positioning. Using mass spectrometry and immunoprecipitation, we identified casein kinase I (CK1) in complex with FAM110A during mitosis. CK1 phosphorylates the C-terminal domain of FAM110A in vitro, and inhibition of CK1 reduces phosphorylation of mitotic FAM110A. Wild-type FAM110A, but not the FAM110A-S252-S255A mutant deficient in CK1 phosphorylation, rescues the chromosomal alignment, duration of mitosis, and orientation of the mitotic spindle after depletion of endogenous FAM110A. We propose that CK1 regulates chromosomal alignment by phosphorylating FAM110A and promoting its interaction with mitotic spindle.

Keywords casein kinase 1; cell cycle; chromosomal alignment; G2 phase; mitosis

Subject Categories Cell Adhesion, Polarity & Cytoskeleton; Cell Cycle

DOI 10.15252/embr.202051847 | Received 9 October 2020 | Revised 14 April 2021 | Accepted 5 May 2021 | Published online 26 May 2021

EMBO Reports (2021) 22: e51847

Introduction

Progression through the cell cycle is driven by cyclin-dependent kinases (CDK) that act in complex with various cyclins, including cyclin D and E in G1, cyclin A in S/G2, and cyclin B in G2/M phases of the cell cycle (Malumbres & Barbacid, 2009). CDK activity triggers periodical changes in transcription during progression through the cell cycle. Phosphorylation of the retinoblastoma-associated protein RB1 by cyclin D-CDK4/6 in G1 phase allows activation of the E2F family transcription factors leading to production of cyclin E-CDK2 and promoting G1/S transition (van den Heuvel & Dyson, 2008; Bertoli *et al,* 2013). Premature expression of mitosis-promoting genes is suppressed by a DREAM complex binding to CHR elements in the promoters (Müller *et al,* 2014). Transcription factors B-MYB and FOXM1 are sequentially recruited to the DREAM complex in G2 and promote expression of the G2/M genes (Laoukili *et al,* 2005; Sadasivam *et al,* 2012). Phosphorylation of B-MYB and FOXM1 by CDKs is needed for activation of their transactivation domains and full expression of the G2/M genes (Saville & Watson, 1998; Laoukili *et al,* 2008). FOXM1 promotes expression of multiple proteins including cyclin B (CCNB1), polo-like kinase 1 (PLK1), dual specificity phosphatases (CDC25B and CDC25C), and Aurora kinase B (AURKB) that play essential roles in mitotic entry, organization of the bipolar mitotic spindle, sister chromatid segregation, and cytokinesis (Laoukili *et al,* 2005).

Periodical expression of genes in individual phases of the cell cycle has been widely studied in several models including yeast and human transformed cell lines (Cho *et al,* 1998; Chaudhry *et al,* 2002; Whitfield *et al,* 2002; Rustici *et al,* 2004; Grant *et al,* 2013). Such transcriptomic analysis typically requires cell synchronization by various techniques including inhibition of DNA replication by thymidine or blocking mitotic progression by a microtubule-depolymerizing drug nocodazole (Ma & Poon, 2011). Although these techniques efficiently enrich cells in certain cell cycle phase, they also generate substantial level of cellular stress that may affect gene expression and generate artifacts in evaluation of differences between individual phases of the cell cycle (Shedden & Cooper, 2002; Cooper & Shedden, 2003; Grant *et al,* 2013). For instance, treatment with thymidine arrests cells at the beginning of S phase but also invariably leads to activation of ATM and ATR kinases (Bolderson *et al,* 2004; Halicka *et al,* 2017). Activation of the p53 pathway leads to expression of the CDK inhibitor p21/CDKN1A that affects expression of multiple cell cycle genes (de Toledo *et al,* 1998; Löhr *et al,* 2003; Fischer *et al,* 2016). Similarly, prolonged prometaphase block caused by nocodazole activates mitogen-activated protein kinase p38 and this may affect progression through the subsequent interphase (Takenaka *et al,* 1998; Uetake & Sluder, 2010).

Cancer Cell Biology, Institute of Molecular Genetics of the Czech Academy of Sciences, Prague, Czech Republic
*Corresponding author. Tel: +420 241063210; E-mail: libor.macurek@img.cas.cz

Casein kinase I (CK1) is a family of seven monomeric serine/threonine protein kinases implicated in various cellular functions including WNT signaling, nucleo-cytoplasmic transport, circadian rhythms, DNA repair, and mitosis (Knippschild *et al,* 2005; Johnson Alyssa *et al,* 2013; Cruciat, 2014). In mitosis, various CK1 isoforms were reported to localize at spindle poles and CK1 was also identified as a component of mitotic spindles by proteomic screens (Milne *et al,* 2001; Sauer *et al,* 2005; Peng *et al,* 2015). A coiled-coil anchoring protein AKAP450 has been reported to recruit CSNK1D to the spindle poles, whereas localization of CSNK1A is mediated by its interaction with FAM83D (also known as spindle protein CHICA; Sillibourne *et al,* 2002; Santamaria *et al,* 2008; Fulcher *et al,* 2018; Fulcher *et al,* 2019). Inhibition of CK1 using small-molecule inhibitors caused mitotic defects (Behrend *et al,* 2000; Cheong *et al,* 2011). CK1 was implicated in positioning of the mitotic spindle in yeast, worms, and human cells (Panbianco *et al,* 2008; Peng *et al,* 2015; Portegijs *et al,* 2016; Fulcher *et al,* 2019). In *C. elegans* embryos, CK1 activity controls asymmetric distribution of the Gα, GPR-1/2, and LIN-5 complex (Gα-LGN-NuMA in mammals) that mediates binding of the astral microtubules to actin-rich cell cortex and thus regulates positioning of the mitotic spindle (Panbianco *et al,* 2008). In addition, phosphorylation of LIN-5 by CK1 promotes its interaction with GPR-1/2 and contributes to the cortical pulling forces on mitotic spindle (Portegijs *et al,* 2016). In human cells, recruitment of dynein to the LGN-NuMA is restricted by polo-like kinase 1 (PLK1) localized at the spindle poles (Kiyomitsu & Cheeseman, 2012). In addition, cortical enrichment of the LGN-NuMA is suppressed by Ran-GTP and PLK1 activities resulting from a close proximity of misaligned chromosomes in the cell cortex (Kiyomitsu & Cheeseman, 2012; Tame *et al,* 2016). Cortical localization of NuMA is negatively regulated during metaphase through its phosphorylation by CDK1, PLK1, and Aurora-A (Kotak *et al,* 2013; Seldin *et al,* 2013; Gallini *et al,* 2016; Kotak *et al,* 2016; Sana *et al,* 2018). Finally, CK1 was also implicated in spindle positioning in human cells, yet its substrates still remain to be determined (Fulcher *et al,* 2019).

Here, we compared gene expression in G1 and G2 cells sorted from asynchronously growing human non-transformed cells based on expression of a fluorescent ubiquitination-based cell cycle indicator and identified 701 differentially expressed transcripts (Sakaue-Sawano *et al,* 2008; Sakaue-Sawano *et al,* 2017). Further, we characterized the family with sequence similarity 110 member A (FAM110A, also reported as C20orf55) that showed high expression in G2 cells. We have observed that FAM110A localizes at the spindle poles during mitosis and that depletion of FAM110A by RNAi causes mitotic defects. Impaired chromosomal alignment in FAM110A-depleted cells delayed entry to anaphase, extended duration of mitosis, and impaired orientation of the mitotic spindle. Mass spectrometry and immunoprecipitation revealed interaction of the mitotic FAM110A with actin, tubulin, and CK1 family protein kinases CSNK1D/E. In addition, we found that CK1 kinase phosphorylated the C-terminal domain of FAM110A in mitosis. EGFP-FAM110A mutants deficient in CK1 binding or CK1-mediated phosphorylation failed to rescue the loss of endogenous FAM110A. We propose that phosphorylation of FAM110A by CK1 regulates its localization to mitotic spindle and is required for correct chromosomal alignment.

Results

Screen for G2/M-expressed genes in human non-transformed cells

We aimed here to identify potential new regulators of the cell cycle and mitosis by comparing gene expression in human non-transformed cells in various phases of the cell cycle. To avoid the impact of cell synchronization on the gene expression, we established RPE-FUCCI cell line that allows efficient isolation of G1, S, and G2/M cells from asynchronously growing cell cultures (Sakaue-Sawano *et al,* 2008; Sakaue-Sawano *et al,* 2017). In agreement with previous reports, we found that cells positive for RFP and negative for GFP signal are dominantly in G1 phase, cells positive for GFP and negative for RFP in G2 phase, and double positive cells in S phase (Fig 1A). Next, we performed expression profiling of the parental cell population and isolated G1 and G2 cells. As expected, we found significant enrichment of *CCNE1* mRNA in G1 cells as well as enrichment of *CCNA2* and *CCNB1* in G2 cells (Pines & Hunter, 1989; Pagano *et al,* 1992; Baldin *et al,* 1993; Ohtsubo *et al,* 1995). In G2 cells, we observed high enrichment of mitotic kinases *MPS1/TTK*, *PLK1, AURKA,* and its cofactor *BORA*; centromeric histones *CENPA*, *CENPF*, *CENPE*, and *INCENP*; kinetochore proteins *NDC80* and *NUF2*; microtubule motor proteins *KIF2C, KIF14,* and *KIF18A*; and component of APC/C ubiquitin ligase complex *UBE2C,* that are jointly involved in mitotic entry, organization of the mitotic spindle, and segregation of sister chromatids during mitosis (Lindqvist *et al,* 2009; Hara & Fukagawa, 2018; Srivastava *et al,* 2018; Vigneron *et al,* 2018). G2 cells also expressed high level of topoisomerase *TOP2A* and DNA helicase *PIF1* required for DNA decatenation and for releasing G-quadruplex DNA structures, respectively (Isaacs *et al,* 1998; Dewar & Lydall, 2010; Dahan *et al,* 2018). In summary, we identified 701 transcripts that were significantly differentially expressed between G2 and G1 cells ($q < 0.05$, fold change > 2) (Fig 1B, Dataset EV1). We followed by confirming the differential expression of selected transcripts in GFP^+, RFP^+, and doubly positive RPE-FUCCI cells using quantitative real-time PCR analysis (Fig 1C). As expected, we observed intermediate level of *CCNA2* expression in S phase cells, followed by further increase in G2 cells. Similarly, several of the tested transcripts including *FAM110A*, *FAM72D*, *G2E3,* and *CDCA2* showed gradual increase in expression toward the G2. In contrast, other transcripts including *PIF1* and *NEURL1b* showed an increased expression exclusively in G2 cells. We conclude that RPE-FUCCI cells represent a powerful tool for monitoring gene expression in various cell cycle phases in human non-transformed cells.

FAM110A is highly expressed in G2 and localizes at mitotic spindle during mitosis

Aiming to identify potential new regulators of the cell cycle and mitosis, we selected a previously unexplored FAM110A for further analysis. First, we used siRNA-mediated depletion of FAM110A to test three commercial antibodies and found that all of them specifically recognized FAM110A in immunoblotting (Fig 2A). To complement the analysis of the asynchronously growing FUCCI cells, we synchronized the parental RPE cells at G1/S transition using thymidine, released them to fresh media containing nocodazole, and collected at 2-h intervals. We found that FAM110A was present at

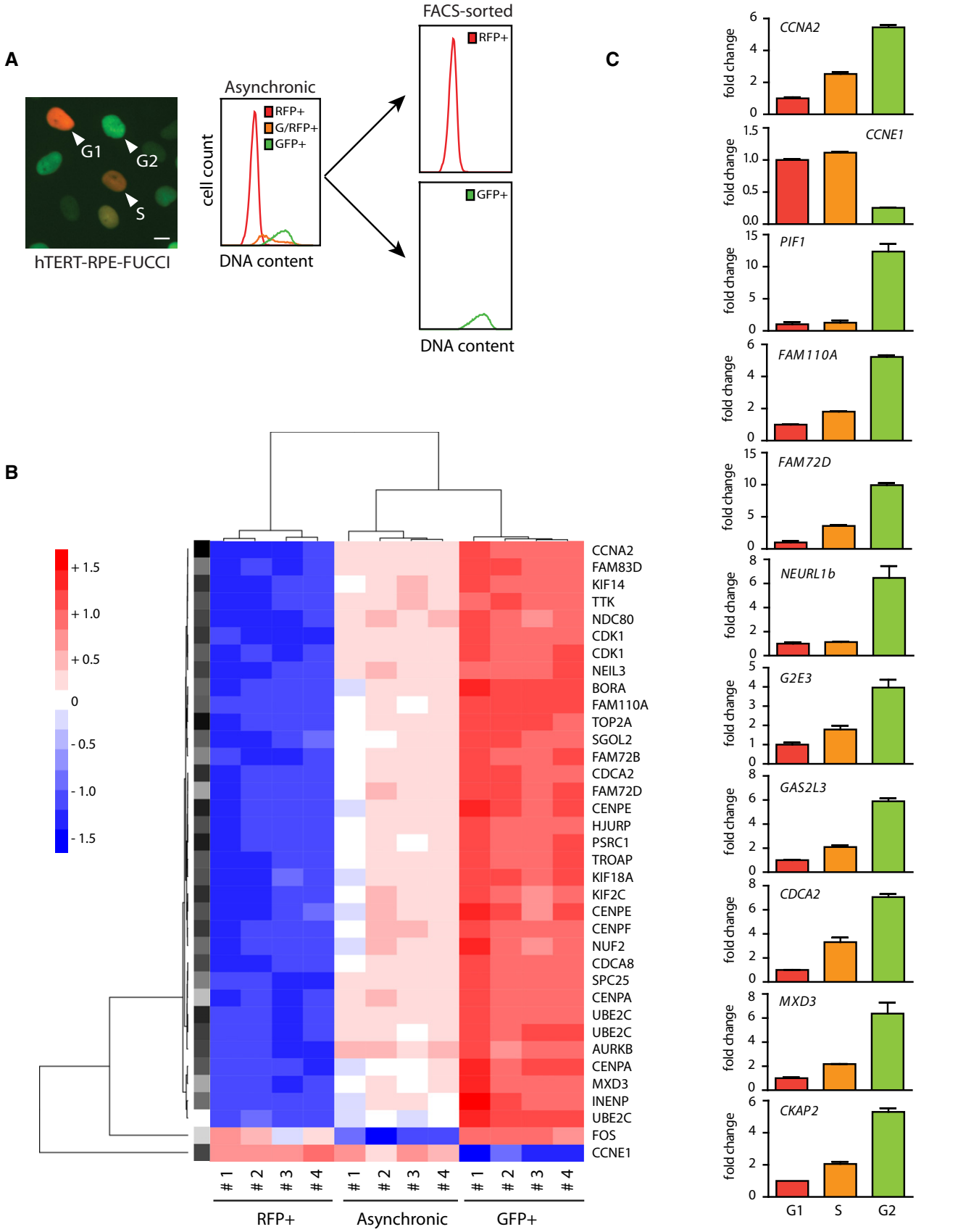
A
G1
G2
S
hTERT-RPE-FUCCI
Asynchronic
RFP+
G/RFP+
GFP+
cell count
DNA content
FACS-sorted
RFP+
GFP+
DNA content
B
+ 1.5
+ 1.0
+ 0.5
0
- 0.5
- 1.0
- 1.5
CCNA2
FAM83D
KIF14
TTK
NDC80
CDK1
CDK1
NEIL3
BORA
FAM110A
TOP2A
SGOL2
FAM72B
CDCA2
FAM72D
CENPE
HJURP
PSRC1
TROAP
KIF18A
KIF2C
CENPE
CENPF
NUF2
CDCA8
SPC25
CENPA
UBE2C
UBE2C
AURKB
CENPA
MXD3
INENP
UBE2C
FOS
CCNE1
1
2
3
4
RFP+
Asynchronic
GFP+
C
CCNA2
CCNE1
PIF1
FAM110A
FAM72D
NEURL1b
G2E3
GAS2L3
CDCA2
MXD3
CKAP2
fold change
G1
S
G2

Figure 1.

Figure 1. Screen for cell cycle-regulated genes using RPE-FUCCI cells.

A Schematic of flow cytometry sorting of RFP^+ and GFP^+ cells from asynchronously growing RPE-FUCCI cells. DAPI was used to probe for DNA content. Representative image of FUCCI cells imaged by immunofluorescence microscopy is shown on the left. Scale bar indicates 10 μm.

B RNA was isolated from asynchronic RPE-FUCCI cells and RFP^+ (G1 phase) and GFP^+ (G2 phase) cells and analyzed using Illumina HumanHT-12 v4 Expression BeadChip ($n = 4$). Shown are 36 transcripts with fold change expression > 8 between G2 and G1 cells and $q < 0.05$. Color scale of the row Z score is shown on the left.

C RFP^+ (G1 phase), GFP^+ (G2 phase), and GFP^+/RFP^+ (S phase) RPE-FUCCI cells were sorted by flow cytometry, and RNA was extracted and analyzed using qRT–PCR ($n = 3$). Expression is normalized to *GAPDH* mRNA. Bars show mean ± SD.

basal levels in G1/S-arrested cells and its expression increased toward mitosis (Fig 2B). We also noted slower migration of FAM110A at SDS–PAGE that was most prominent in cells collected by the mitotic shake-off (Fig 2B). This mobility shift did not occur when entry to mitosis was prevented by RO3306 treatment and conversely it disappeared when cells exited from mitosis after release of the nocodazole block suggesting that FAM110A might be phosphorylated during mitosis and dephosphorylated at mitotic exit (Fig 2B and C). Interestingly, one of the monoclonal antibodies against FAM110A failed to recognize the slowly migrating band in immunoblotting suggesting that it recognizes only the non-phosphorylated epitope (Fig 2B). Further, we immunoprecipitated endogenous FAM110A from cells synchronized in G2 or in mitosis and incubated with mock or with a lambda phosphatase (Fig 2D). Increased mobility of FAM110A treated with lambda phosphatase confirmed that FAM110A is phosphorylated during mitosis. Similar enrichment of FAM110A levels in G2 cells and the mobility shift in mitotic cells was observed also in synchronized U2OS and HeLa cells indicating that FAM110A is cell cycle-regulated also in other cell types (Fig EV1A and B).

To assay distribution of endogenous FAM110A during mitosis, we performed confocal microscopy. Using the rabbit polyclonal antibody, we observed that FAM110A was diffusely distributed in the cytosol in interphase cells and was enriched at the centrosome. In addition, the antibody showed a nuclear staining in interphase cells. In mitotic RPE and U2OS cells, endogenous FAM110A localized to the spindle poles and proximal spindle microtubules which is consistent with a previously reported distribution of EGFP-FAM110A (Figs 2E and EV1C) (Hauge *et al,* 2007). Importantly, the signal at spindle poles was strongly reduced in cells transfected with FAM110A siRNA confirming the specificity of the antibody in mitotic cells (Fig 2E and F). Similarly, the cytoplasmic signal was reduced in interphase cells transfected with FAM110A siRNA. In contrast, the nuclear signal observed in interphase cells persisted after depletion of the FAM110A suggesting that it represents a non-specific component recognized by the polyclonal antibody (Figs 2E and EV1C). Similar but weaker staining of the mitotic spindle poles was observed also by a monoclonal FAM110A antibody clone B11, possibly reflecting the ability of the antibody to recognize only a non-phosphorylated protein (Fig EV1D). Ectopic expression of a homologue FAM110C was previously reported to trigger formation of microtubule bundles and to impair cell morphology (Hauge *et al,* 2007). Here, we generated RPE cells stably expressing mouse EGFP-FAM110A and found a comparable distribution during mitosis as the endogenous FAM110A (Figs 2G and EV1E). Importantly, we did not observe any defects in organization of mitotic spindles indicating that mild expression of exogenous EGFP-FAM110A is well tolerated in the stable cell line. In addition, we observed that EGFP-FAM110A was also enriched in the cell cortex throughout mitosis (Fig EV1E).

Depletion of FAM110A slows down mitotic progression and leads to mitotic defects

To analyze the role of FAM110A in the cell cycle progression, we used flow cytometry and compared distribution of the cells transfected with control or FAM110A siRNA (Fig 3A). We found that depletion of FAM110A with two independent siRNAs led to accumulation of cells with 4 N DNA content. More specifically, we observed 70% increase of the mitotic fraction in FAM110A-depleted cells compared to the control cells suggesting that FAM110A might play role during mitotic progression (Fig 3A and B). In agreement with this, we observed an increased level of histone H3 phosphorylated at Ser10 (pS10-H3; mitotic marker) in cells with depleted FAM110A (Fig 3C). Interestingly, depletion of CSPP1 did not increase the mitotic index and the pS10-H3 signal suggesting that FAM110A regulates mitosis through another mechanism than through its previously reported interacting partner CSPP1 (Fig 3B and C; Patzke *et al,* 2005; Hauge *et al,* 2007). Importantly, depletion of the endogenous FAM110A in cells expressing the mouse EGFP-FAM110A did not increase the level of the mitotic markers pS10-H3 and pMPM2 in immunoblotting and flow cytometry, respectively, confirming the specificity of the siRNA (Fig 3D). Next, we scored the mitotic defects in control or FAM110A siRNA-transfected cells and found that depletion of FAM110A significantly increased the fraction of cells with aberrant chromosome alignment in metaphase (Fig 3E). In addition, cells depleted of FAM110A showed significantly increased number of multipolar mitotic spindles compared to control cells, although the majority of spindles remained bipolar (Fig 3E). Compared to the control cells, we also observed frequent lagging chromosomes in anaphase cells depleted of FAM110A (Fig 3F).

To uncover the mitotic defect caused by depletion of FAM110A, we performed live imaging of asynchronously growing U2OS-H2B-gfp cells transfected with control or FAM110A siRNA and measured the time from nuclear envelope breakdown to anaphase (Fig 4A and B). We observed that depletion of FAM110A significantly increased the time required for initiation of anaphase (Fig 4C). In addition, we noticed that a fraction of cells with depleted FAM110A failed to segregate the chromosomes and died during the experiment or progressed to the G1 with severely impaired nuclear organization (Fig 4D). We conclude that depletion of FAM110A extends duration of mitosis most probably due to defects in mitotic spindle organization causing impaired chromosomal alignment in metaphase.

FAM110A interacts with casein kinase 1 during mitosis

To identify the mechanism by which FAM110A might influence mitotic progression, we performed mass spectrometry analysis of proteins interacting with FAM110A (Fig 5A, Dataset EV2). To this end, we arrested RPE cells stably expressing EGFP or EGFP-FAM110A

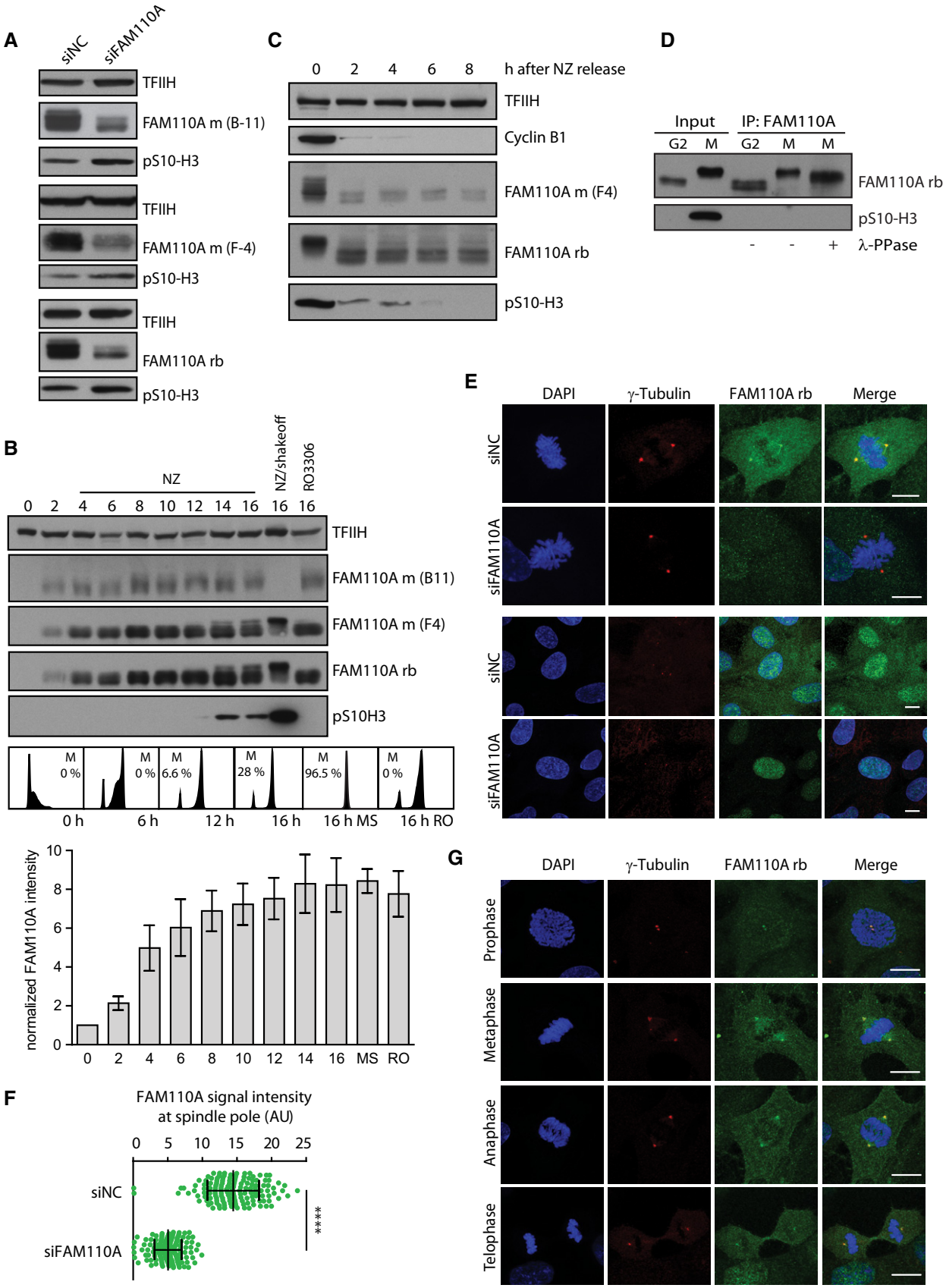
A
siNC
siFAM110A
TFIIH
FAM110A m (B-11)
pS10-H3
TFIIH
FAM110A m (F-4)
pS10-H3
TFIIH
FAM110A rb
pS10-H3
C
0 2 4 6 8 h after NZ release
TFIIH
Cyclin B1
FAM110A m (F4)
FAM110A rb
pS10-H3
D
Input
IP: FAM110A
G2 M G2 M M
FAM110A rb
pS10-H3
- - + λ-PPase
B
NZ
NZ/shakeoff
RO3306
0 2 4 6 8 10 12 14 16 16 16
TFIIH
FAM110A m (B11)
FAM110A m (F4)
FAM110A rb
pS10H3
M 0 %
M 0 %
M 6.6 %
M 28 %
M 96.5 %
M 0 %
0 h
6 h
12 h
16 h
16 h MS
16 h RO
normalized FAM110A intensity
0 2 4 6 8 10 12 14 16 MS RO
E
DAPI
γ-Tubulin
FAM110A rb
Merge
siNC
siFAM110A
siNC
siFAM110A
F
FAM110A signal intensity at spindle pole (AU)
0 5 10 15 20 25
siNC
siFAM110A
****
G
DAPI
γ-Tubulin
FAM110A rb
Merge
Prophase
Metaphase
Anaphase
Telophase

Figure 2.

Figure 2. Expression of FAM110A increases toward mitosis.

A RPE cells were transfected with control or FAM110A siRNA, whole-cell lysates were prepared after 48 h, and indicated antibodies were tested in immunoblotting.

B RPE cells were released for indicated times from a thymidine block, and collected cells were analyzed by immunoblotting and FACS. Nocodazole was added after 4 h to arrest cells in mitosis. Alternatively, RO3306 inhibitor was added to prevent mitotic entry. Where indicated, sample was collected by mitotic shake-off (MS) to obtain pure mitotic population. Samples were analyzed by immunoblotting (upper panel). Staining for pS10-H3 was used as a marker of mitosis and TFIIH as a loading control. In parallel, cell cycle progression was followed by flow cytometry using DAPI and mpm2 staining. Representative plot is shown, and M indicates percentage of mitotic cells (middle panel). Signal of the rabbit FAM110A antibody was quantified in three independent replicates and normalized to the loading and to the thymidine arrested sample (lower panel). Bars show median ± SD.

C RPE cells were arrested in mitosis by nocodazole, collected by mitotic shake-off, and released to fresh media for indicated times to allow mitotic exit. Loss of pS10-H3 signal was used as a marker of mitotic exit.

D RPE cells arrested in G2 by RO3306 (G2) or in mitosis (M) by nocodazole treatment were extracted and endogenous FAM110A was immunoprecipitated using rabbit polyclonal antibody immobilized on pA/G beads. Beads were incubated with mock or with lambda phosphatase for 20 min at 30°C. Proteins were separated by SDS–PAGE and detected by immunoblotting.

E RPE cells transfected with control or FAM110A siRNA were fixed with 4% PFA, probed with rabbit polyclonal antibody against FAM110A and mouse monoclonal to γ-tubulin, and were analyzed by confocal microscopy. Shown is maximal projection of representative mitotic (upper panel) and interphase (lower panel) cells. Scale bars indicate 10 μm.

F Quantification of the signal at spindle poles from (E). Signal intensity of the rabbit polyclonal antibody to FAM110A was determined in regions positive for γ-tubulin. Each dot represents a single spindle pole. Bars show median ± SD. Significance was evaluated by a *t*-test ($n = 3$), ****$P < 0.0001$.

G Asynchronously growing RPE cells were fixed and probed with the rabbit polyclonal antibody to FAM110A. Shown are representative images of cells in various phases of mitosis. Individual z-stacks were de-convoluted using Huygens Deconvolution Software, processed sequentially, and are presented as maximum projections. Scale bars indicate 10 μm.

Source data are available online for this figure.

in mitosis by treating them with nocodazole, isolated interacting proteins using GFP-Trap, and identified them by mass spectrometry. Among the strongest hits, we identified actin and α/β-catenin suggesting that FAM110A might be associated with actin cytoskeleton and cell adhesion molecules. Proteomic analysis also revealed specific interaction between FAM110A and tubulin. Enrichment of tubulin in complex with the EGFP-FAM110A was lower than that of actin, possibly reflecting microtubule depolymerization in the presence of nocodazole used for synchronization of the cells. In addition, we identified casein kinase 1 isoforms epsilon (CSNK1E or CK1ε) and delta (CSNK1D or CK1δ) as interacting partners of mitotic FAM110A (Fig 5A). To validate the proteomic analysis, we immunoprecipitated EGFP or EGFP-FAM110A from asynchronously growing or mitotic cells and analyzed the interacting proteins using immunoblotting (Fig 5B). We found that CSNK1D and CSNK1E formed complex with FAM110A in asynchronic cells and that this interaction was further increased during mitosis (Fig 5B). Inversely, we immunoprecipitated endogenous CSNK1D or CSNK1E and confirmed a strong interaction with EGFP-FAM110A during mitosis (Fig 5C and EV2A).

Next, we mapped the interaction between the EGFP-tagged FAM110A, endogenous CSNK1D, and other proteins using immunoprecipitation (Fig 5D). Whereas the FAM110A-ΔPro mutant lacking the Proline-rich domain pulled down comparable amount of CSNK1D as the wild-type FAM110A, deletion of the C-terminal domain impaired the interaction between FAM110A and CSNK1D (Fig 5D and E). Conversely, the C-terminal domain of FAM110A (but not the N-terminal domain) was sufficient to interact with CSNK1D (Fig 5D and E). Within the C-terminal domain, we identified a short peptide sequence resembling a previously reported F-X-X-X-F consensus docking motif for CK1 (Okamura *et al,* 2004; Fulcher *et al,* 2018). Similarly as deletion of the whole C-terminal domain, mutagenesis of the F205, F206, and F208 residues to alanines impaired interaction of the EGFP-FAM110A-FA with CSNK1D (Fig 5F). Notably, the wild-type FAM110A co-immunoprecipitated with tubulin, whereas the interaction was lost in FAM110A-ΔC mutant suggesting that tubulin binds to the C-terminal domain of FAM110A (Fig 5E). In contrast, we found that deletion of the C-terminal domain did not affect the interaction with catenin and actin, whereas the N-terminal domain of FAM110A was sufficient to mediate the binding (Fig 5E and EV2B). We conclude that binding of tubulin and actin is mediated by distinct regions of the FAM110A.

C-terminal domain of FAM110A is phosphorylated by CK1 in mitosis

To identify protein kinases that control FAM110A phosphorylation in mitosis, we treated mitotic RPE cells with selective small-molecule inhibitors and tested their impact on electrophoretic mobility of endogenous FAM110A. As expected, treatment of cells by PLK1 inhibitor BI2536 increased the mobility of Cdc27 (Fig 6A; Kraft *et al,* 2003; Lénárt *et al,* 2007). Similarly, treatment with Aurora-A inhibitor MLN8054 prevented auto-phosphorylation of Aurora-A at T288 (Fig 6A) (Manfredi *et al,* 2007). However, under same conditions, we did not observe any impact of PLK1 and Aurora-A inhibition on the mobility of FAM110A (Fig 6A). In contrast, treatment with a CDK1 inhibitor resulted in disappearance of the slowly migrating band indicating that CDK1 might phosphorylate FAM110A during mitosis (Fig 6A). Consistent with this possibility, we found that CDK1/cyclin B was able to phosphorylate FAM110A *in vitro* (Fig 6B). On the other hand, we cannot rule out that RO3306 treatment impacted on FAM110A phosphorylation also indirectly as the inhibition of CDK1 forced mitotic exit (Fig 6A). As the proteomic analysis revealed a strong interaction between FAM110A and CK1, we asked whether CK1 could be responsible for mitotic modification of FAM110A. Indeed, we found that treatment of cells with a CK1 inhibitor PF670462 affected the mobility of mitotic FAM110A without inducing mitotic exit in both RPE and U2OS cells (Fig 6A and G; Badura *et al,* 2007; Keenan *et al,* 2018). Interestingly, treatment with PF670462 partially restored the ability of B11 antibody to recognize FAM110A, which is consistent with its dephosphorylation. To validate the data obtained by the inhibitor treatment, we depleted two isoforms of CK1 and tested the impact on the mobility of mitotic

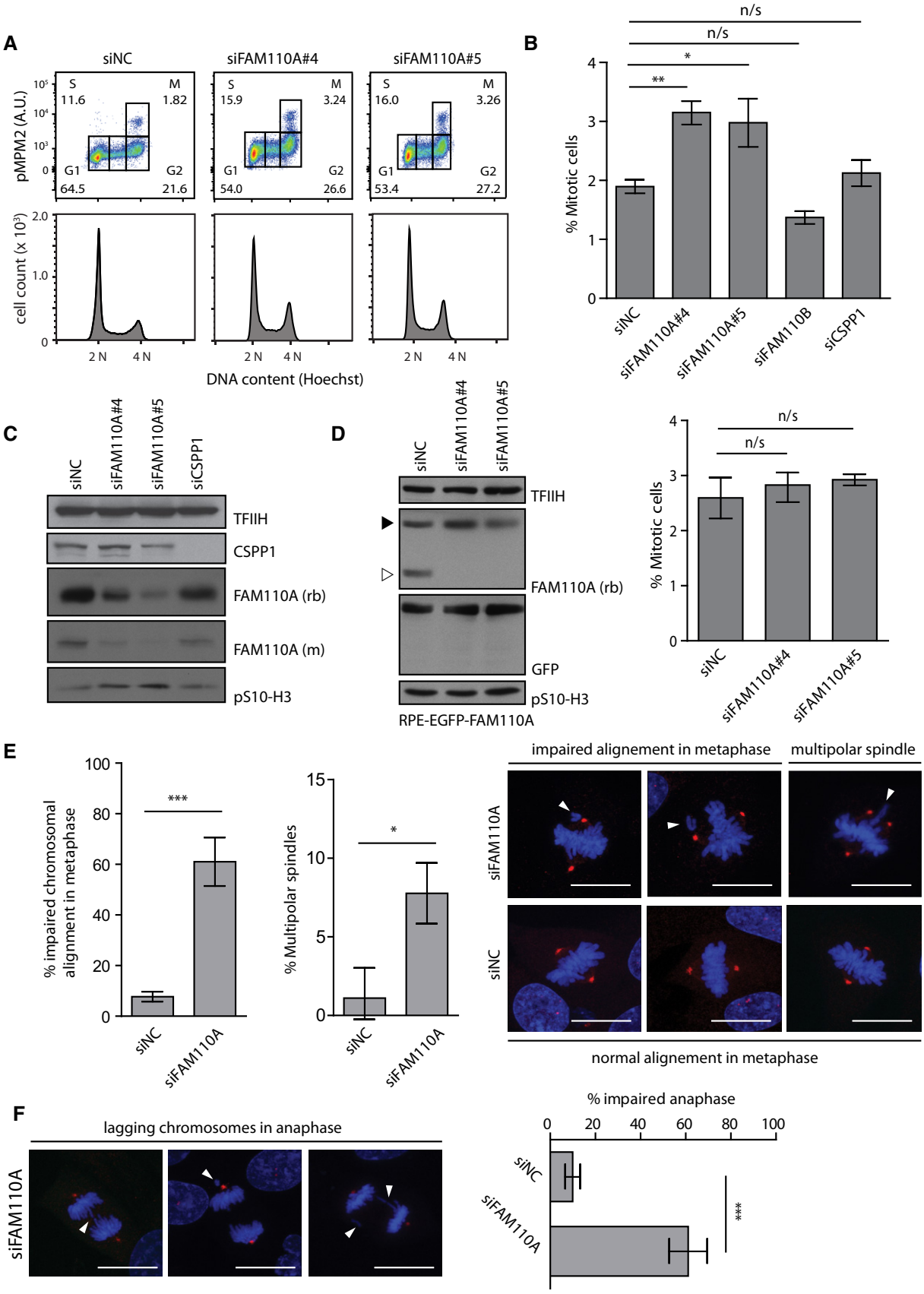
A
siNC
siFAM110A#4
siFAM110A#5
pMPM2 (A.U.)
S 11.6
M 1.82
G1 64.5
G2 21.6
S 15.9
M 3.24
G1 54.0
G2 26.6
S 16.0
M 3.26
G1 53.4
G2 27.2
cell count (x 10³)
2 N
4 N
DNA content (Hoechst)
B
n/s
n/s
*
**
% Mitotic cells
siNC
siFAM110A#4
siFAM110A#5
siFAM110B
siCSPP1
C
siNC
siFAM110A#4
siFAM110A#5
siCSPP1
TFIIH
CSPP1
FAM110A (rb)
FAM110A (m)
pS10-H3
D
siNC
siFAM110A#4
siFAM110A#5
TFIIH
FAM110A (rb)
GFP
pS10-H3
RPE-EGFP-FAM110A
n/s
n/s
% Mitotic cells
siNC
siFAM110A#4
siFAM110A#5
E
% impaired chromosomal alignment in metaphase
***
siNC
siFAM110A
% Multipolar spindles
*
siNC
siFAM110A
impaired alignement in metaphase
multipolar spindle
siFAM110A
siNC
normal alignement in metaphase
F
lagging chromosomes in anaphase
siFAM110A
% impaired anaphase
siNC
siFAM110A
***

Figure 3.

Figure 3. Depletion of FAM110A impairs progression through mitosis.

A RPE cells transfected with control or FAM110A siRNA were fixed, stained with MPM2 antibody (marker of mitosis) and DAPI, and were analyzed by flow cytometry. Representative graphs are shown. Numbers indicate fractions of individual cell cycle phases and mitotic cells.

B Quantification of the mitotic index in three experiments from (A) and in RPE cells transfected with siRNAs to FAM110B and CSPP1 that were analyzed in parallel. Shown is median ± SD ($n = 3$). Statistical significance was determined by ANOVA (*$P < 0.05$ and **$P < 0.005$).

C RPE cells transfected with control, FAM110A, or CSPP1 siRNAs were collected and analyzed by immunoblotting with indicated antibodies.

D RPE cells stably expressing mouse EGFP-FAM110A were transfected with control or two various FAM110A siRNAs, and whole-cell lysates were analyzed by immunoblotting with indicated antibodies (left panel). Empty arrowhead indicates position of the endogenous FAM110A, filled arrowhead the EGFP-FAM110A. In parallel, mitotic index was determined by flow cytometry. Statistical significance was evaluated by ANOVA ($n = 3$). Bars indicate median ± SD.

E RPE cells transfected with control or FAM110A siRNA were grown for 48 h and treated with MG132 30 min prior fixation to trap mitotic cells in metaphase. Impaired chromosomal alignment and multipolar spindles were scored, and representative images are shown. Scale bars indicate 20 μm, and arrowheads point to misaligned chromosomes. More than 30 metaphases were evaluated per condition ($n = 3$). Bars indicate median ± SD. Statistical significance was determined by two-tailed *t*-test (***$P < 0.001$ and *$P < 0.05$).

F Quantification of lagging chromosomes in anaphase cells from (E). More than 30 anaphases were evaluated per condition ($n = 3$). Representative images of abnormal anaphase are shown, scale bars indicate 20 μm, and arrowheads point to incorrectly segregating chromosomes. Statistical significance was determined by two-tailed *t*-test. Bars indicate median ± SD (***$P < 0.001$).

Source data are available online for this figure.

FAM110A. Depletion of CSNK1D by RNAi impaired mobility of the mitotic FAM110A indicating that CK1 phosphorylates FAM110A during mitosis (Fig 6C). On the other hand, depletion of CSNK1E did not affect the mobility of mitotic FAM110A suggesting that its function in FAM110A modification is redundant and can be substituted by the CSNK1D (Fig 6C). Further, we found that incubation of the wild-type FAM110A with CSNK1D induced a similar mobility shift confirming its ability to phosphorylate FAM110A *in vitro* (Fig 6D). In contrast to CDK1 that phosphorylated a fragment comprising of the N-terminal domain and the Pro-rich loop of the FAM110A, deletion of the C-terminal part impaired the ability of CK1 to phosphorylate FAM110A (Fig 6B and D). We conclude that CK1 phosphorylates the C-terminal part of FAM110A during mitosis. Data from a PhosphoSitePlus database suggested that there were two phosphorylated regions within the C-terminal domain of human FAM110A, namely residues S189–S192 and S252–255, matching a consensus phosphorylation motif for CK1 (Flotow *et al,* 1990; Hornbeck *et al,* 2015). Out of the two motifs, substitution of the S252-255 residues to alanines reduced the mobility shift of the mitotic EGFP-FAM110A (Fig 6E). After incubation with CK1, purified FAM110A-S252-255A mutant showed partially reduced mobility shift and incorporation of the radioactive phosphate compared to the wild-type FAM110A (Fig 6F). Altogether, these data confirm that CK1 phosphorylates mitotic FAM110A at the S252-S255 cluster, although incomplete reduction of the phosphate incorporation observed in the *in vitro* assay suggests that CK1 might phosphorylate additional residues in the C-terminal domain of FAM110A.

Phosphorylation of FAM110A by CK1 controls its function in mitosis

Next, we compared the impact of FAM110A depletion and CK1 inhibition on mitotic progression. We found that similarly to FAM110A depletion, inhibition of CK1 extended the duration of mitosis and caused segregation errors (Fig 7A and EV3A–C). Prolonged mitosis was observed also after depletion of CSNK1D and CSNK1E isoforms individually suggesting they are both involved in regulation of mitotic progression (Appendix Fig S1A and B). Encouraged by this finding, we asked whether the CK1-dependent phosphorylation of FAM110A modulates its function in mitosis. To this end, we generated cell lines stably expressing the wild-type or mutant EGFP-FAM110A and assayed their ability to rescue the loss of endogenous FAM110A (Fig 7B). Time-lapse microscopy and flow cytometry revealed that contrary to the parental RPE cells, cells expressing the wild-type mouse FAM110A progressed through mitosis with normal timing and did not accumulate in mitosis upon depletion of endogenous FAM110A (Figs 7C and EV3D). Similarly, expression of FAM110A-ΔPro mutant rescued the amount of mitotic cells after transfection of FAM110A siRNA suggesting that the Pro-rich region is disposable for mitotic function of FAM110A (Figs 7C and EV3D). In contrast, cells expressing either FAM110A-ΔC, FAM110A-FA, or FAM110A-S252-255A mutants showed significantly increased population of the mitotic cells after depletion of endogenous FAM110A and were delayed in progression through mitosis (Figs 7C and EV3D). Of note, expression of the FAM110A-S189-192A mutant rescued the amount of mitotic cells to similar extent as the wild-type FAM110A and FAM110A-S189-192A properly localized at spindle poles suggesting that S189-192 residues are not involved in control of the mitotic function of FAM110A (Appendix Fig S2A–C). Next, we tested the ability of the FAM110A mutants to rescue the chromosomal alignment in metaphase cells. We found that the wild-type FAM110A rescued the defect upon depletion of endogenous FAM110A but it failed to rescue the defect caused by depletion of CSNK1D (Fig 7D and E). In addition, FAM110A-S252-255A mutant failed to rescue alignment upon depletion of FAM110A or CSNK1D. Conversely, we observed that the phosphorylation-mimicking FAM110A-S252-255E mutant rescued not only depletion of the endogenous FAM110A but also depletion of CSNK1D (Fig 7D and E). Similarly, FAM110A-S252-255E mutant but not the wild-type FAM110A rescued the alignment upon inhibition of CK1 (Fig 7D). We conclude that CSNK1D controls mitotic function of FAM110A through phosphorylation of the S252–255 cluster in the C-terminal domain of FAM110A.

The activity of CK1 has recently been implicated in orientation of mitotic spindle but CK1 substrates present at mitotic spindle have thus far not been identified (Brockman *et al,* 1992; Panbianco *et al,* 2008; Fulcher *et al,* 2019). To investigate possible involvement of FAM110A phosphorylation on spindle orientation, we used U2OS cells stably expressing H2B-GFP and mCherry-tubulin that allowed us to compare the longitudinal axis of the cell with axis of the nuclear division. Whereas direction of the nuclear division typically

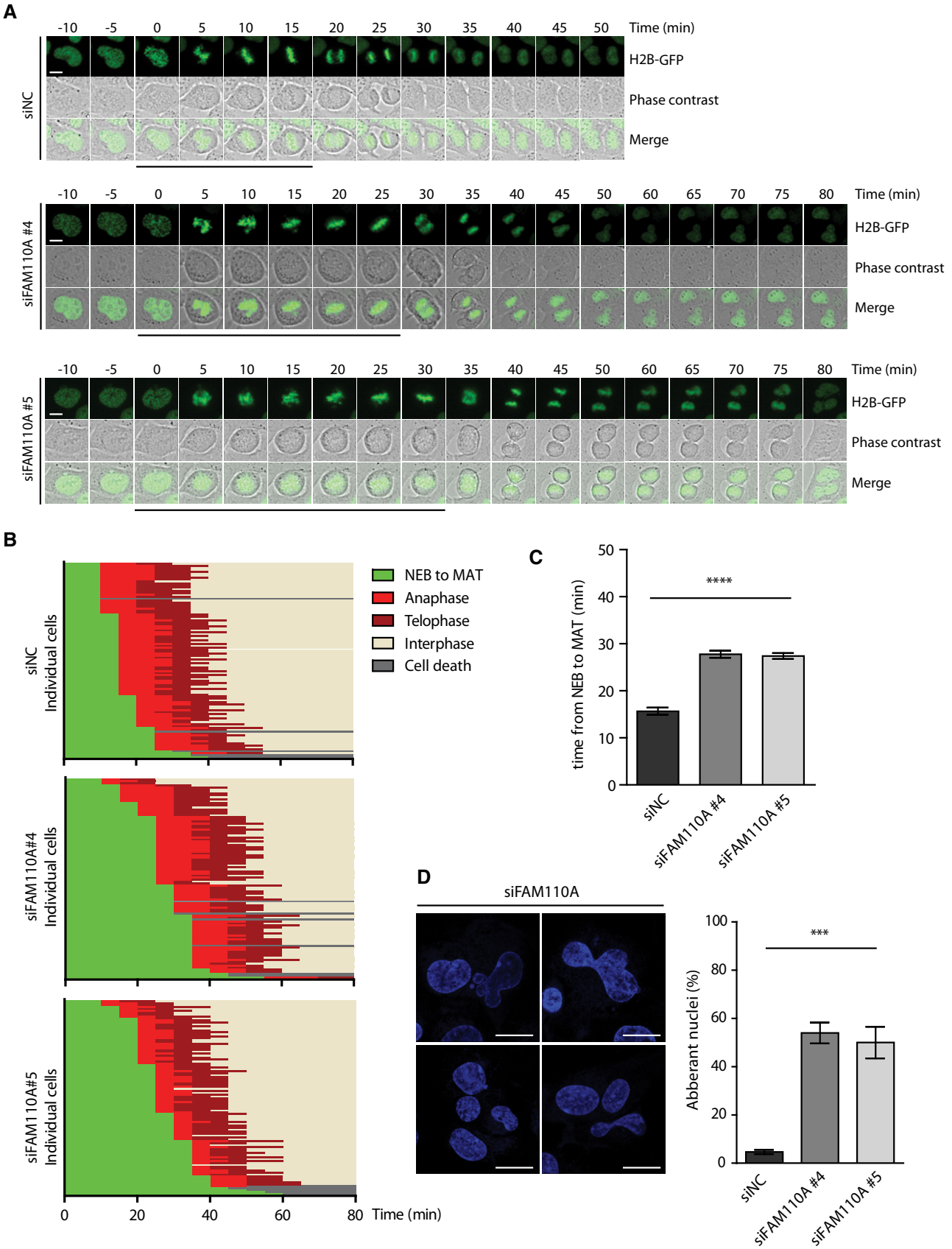

Figure 4.

Figure 4. Depletion of FAM110A delays progression through mitosis.

A U2OS cells stably expressing H2B-EGFP were transfected with indicated siRNAs and after 48 h, they were filmed in 5-min intervals. Time frame closest to the nuclear envelope breakdown (NEB) was set as 0 min. Representative examples are shown ($n = 3$). Black bottom line indicates the time frames from NEB to the metaphase-to-anaphase transition. Scale bars indicate 10 μm.

B Progression through mitosis was categorized in cells from (A) (100/condition) as follows: nuclear envelope breakdown to the metaphase-to-anaphase transition (MAT), anaphase, telophase, and interphase. Data from one of three experiments are shown, and each bar indicates one cell. Cells that died during imaging are shown in gray.

C Time from the nuclear envelope breakdown to MAT was quantified in cells from (B). Shown is median ± SD ($n = 3$). Statistical significance was determined by ANOVA (****$P < 0.0001$).

D Abnormal nuclear organization was scored in cells from (B) that completed cell division. Representative images of aberrant nuclei are shown. Scale bar indicates 15 μm. Plotted is percentage of cells with aberrant nuclei. Shown is median ± SD ($n = 3$). Statistical significance was determined by ANOVA (***$P < 0.001$).

Source data are available online for this figure.

corresponded with the orientation of the cell prior to mitosis in control cells, treatment of cells with PF670462 or depletion of CSNK1D by RNAi increased the proportion of cells exhibiting an increased angle between the nuclear and cellular divisions (Fig EV4A and B; Tame *et al,* 2016; Fulcher *et al,* 2019). Similarly, depletion of FAM110A with two independent siRNAs impaired orientation of the cell division (Fig EV4A and B). To determine whether the observed misoriented cell division was caused by impaired spindle positioning, we measured the angle between the spindle axis and the growth axis (Toyoshima & Nishida, 2007). Indeed, we observed that depletion of CSNK1D or FAM110A increased the spindle angle (Fig EV4C). We performed the same assay in cells stably expressing EGFP-FAM110A or its mutants and found that the wild-type FAM110A fully rescued the increased spindle angle caused by depletion of endogenous FAM110A (Fig 7F). In contrast, cells expressing either FAM110A-ΔC, FAM110A-FA, or FAM110A-S252-255A mutants showed an increased spindle angle (Fig 7F). Similarly, we observed that the wild-type FAM110A, but not FAM110A-ΔC, FAM110A-FA, or FAM110A-S252-255A mutants, rescued the orientation of the cell division (Fig EV4D).

Next, we asked whether CSNK1D controls the spindle orientation through phosphorylation of FAM110A. Whereas expression of the wild-type EGFP-FAM110A rescued the spindle angle after depletion of endogenous FAM110A, it failed to rescue the depletion of CSNK1D (Fig 7G). In contrast, we found that cells expressing the FAM110A-S252-255E mutant showed normal spindle angle after depletion of CSNK1D or its inhibition with PF670462 (Fig 7G). We conclude that FAM110A interaction with and phosphorylation by CSNK1D is needed for proper chromosomal alignment in metaphase allowing correct orientation of mitotic spindle and segregation of sister chromatids along the cellular axis.

Finally, we wished to investigate whether there might be a connection between the chromosomal misalignment observed upon depletion of FAM110A and the spindle orientation defect. Chromosomal fragments present in proximity of the plasma membrane were previously reported to affect localization of LGN during metaphase (Kiyomitsu & Cheeseman, 2012; Tame *et al,* 2016). As expected, metaphase HeLa cells transfected with control siRNA showed correct chromosomal alignment and symmetrical distribution of GFP-LGN. In contrast, we observed displacement of GFP-LGN signal close to the misaligned chromosomes in cells depleted of FAM110A (Fig EV4E). Combined these data suggest that impaired spindle orientation in FAM110A-depleted cells might be caused by misaligned chromosomes triggering displacement of LGN.

CK1-dependent phosphorylation of FAM110A promotes its interaction with mitotic spindle

As the CK1-dependent phosphorylation of FAM110A occurs in the C-terminal domain that mediates interaction with tubulin, we hypothesized that modification of the FAM110A could control its ability to localize to the mitotic spindle. Consistent with this possibility, we found that depletion of CSNK1D impaired the localization of endogenous FAM110A at spindle poles (Fig 8A and B). The amount of FAM110A at spindle poles was further reduced by treating cells with PF670462 possibly reflecting the combined inhibition of CSNK1D and

Figure 5. FAM110A interacts with CK1, tubulin, and actin during mitosis.

A Cell extracts from RPE cells stably expressing EGFP or EGFP-FAM110A arrested in mitosis by nocodazole were incubated with GFP-Trap. Bound proteins were analyzed by mass spectrometry. Shown are top ten proteins that that were significantly enriched in EGFP-FAM110A complex compared to EGFP in three independent experiments. Proteins TUBB8 and TUB1AC were also significantly enriched in complex with EGFP-FAM110A. Number indicates the fold change interaction compared to the control.

B Cell extracts from asynchronously growing or mitotic RPE-EGFP or RPE-EGFP-FAM110A cells were incubated with GFP-Trap, and bound proteins were analyzed by immunoblotting. Antibody against pS10-H3 was used as a marker of mitosis.

C Cell extracts from asynchronously growing or mitotic RPE-EGFP-FAM110A cells were incubated with CSNK1D antibody or control IgG immobilized on protein A/G beads. Bound proteins were probed with antibody against GFP or CK1δ. Staining for pS10-H3 was used as a marker of the mitotic population.

D Scheme of the EGFP-FAM110A constructs used in the study. Numbering is based on human FAM110A. N, C, and Pro represent N-terminal, C-terminal, and Pro-rich domains, respectively.

E Cells were transfected with indicated constructs and after 48 h, they were lysed in RIPA buffer. Cell extracts were immunoprecipitated with GFP-Trap and probed by immunoblotting ($n = 2$).

F Cells were transfected with EGFP, EGFP-FAM110A-WT, or EGFP-FAM110A-FA. Cell extracts were immunoprecipitated with GFP-Trap, and binding of CK1 was determined by immunoblotting ($n = 3$).

Source data are available online for this figure.

A

Protein ID	Gene	Protein	Fold change
Q9BQ89	FAM110A	Protein FAM110A	671
P68133	ACTA1	Actin	216
P49674	CSNK1E	Casein kinase I isoform epsilon	96
P35221	CTNNA1	Catenin alpha-1	80
Q13813	SPTAN1	Spectrin alpha chain, non-erythrocytic 1	43
P35222	CTNNB1	Catenin beta-1	42
Q13049	TRIM32	E3 ubiquitin-protein ligase TRIM32	41
P62258	YWHAE	14-3-3 protein epsilon	41
O43707	ACTN4	Alpha-actinin-4	40
P48730	CSNK1D	Casein kinase I isoform delta	23
...		...	
Q3ZCM7	TUBB8	Tubulin beta-8	9
Q9BQE3	TUBA1C	Tubulin alpha-1C	7

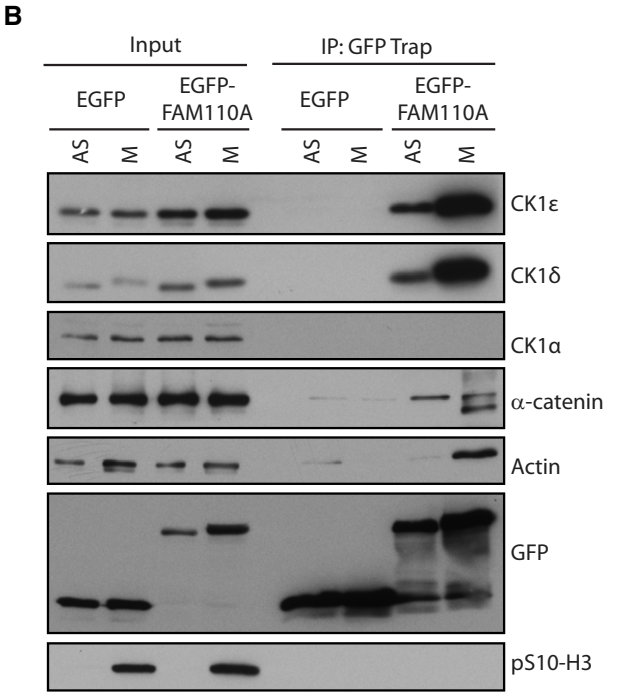

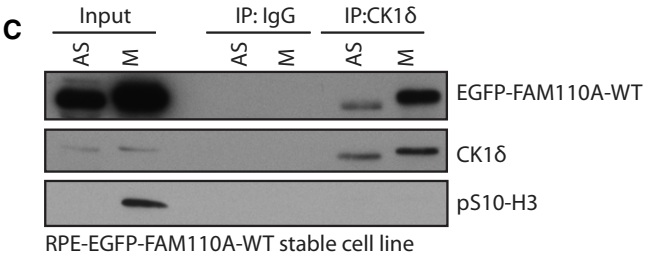

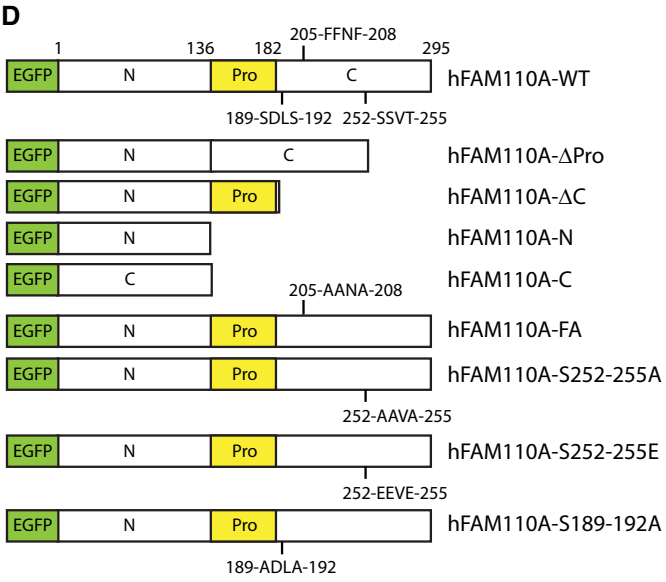

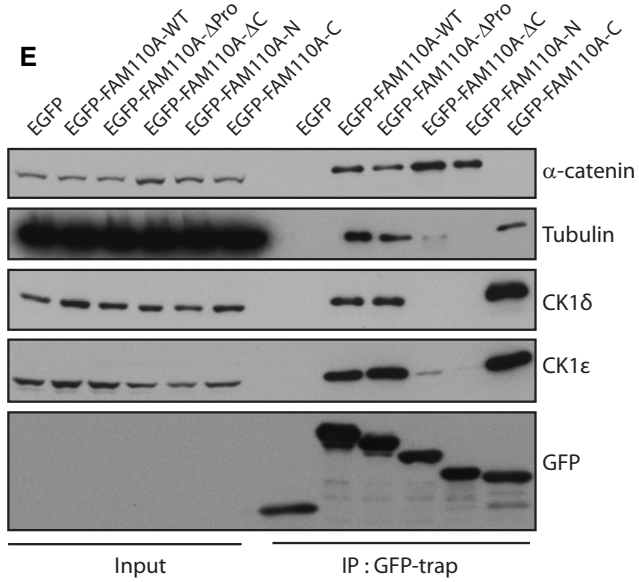

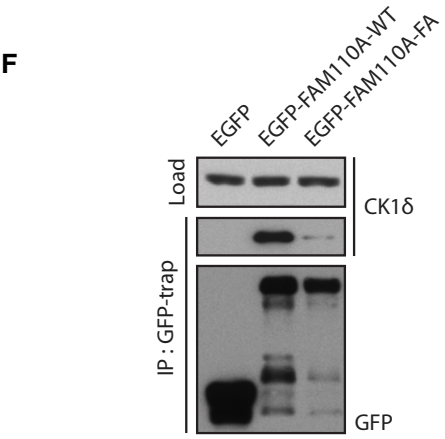

Figure 5.

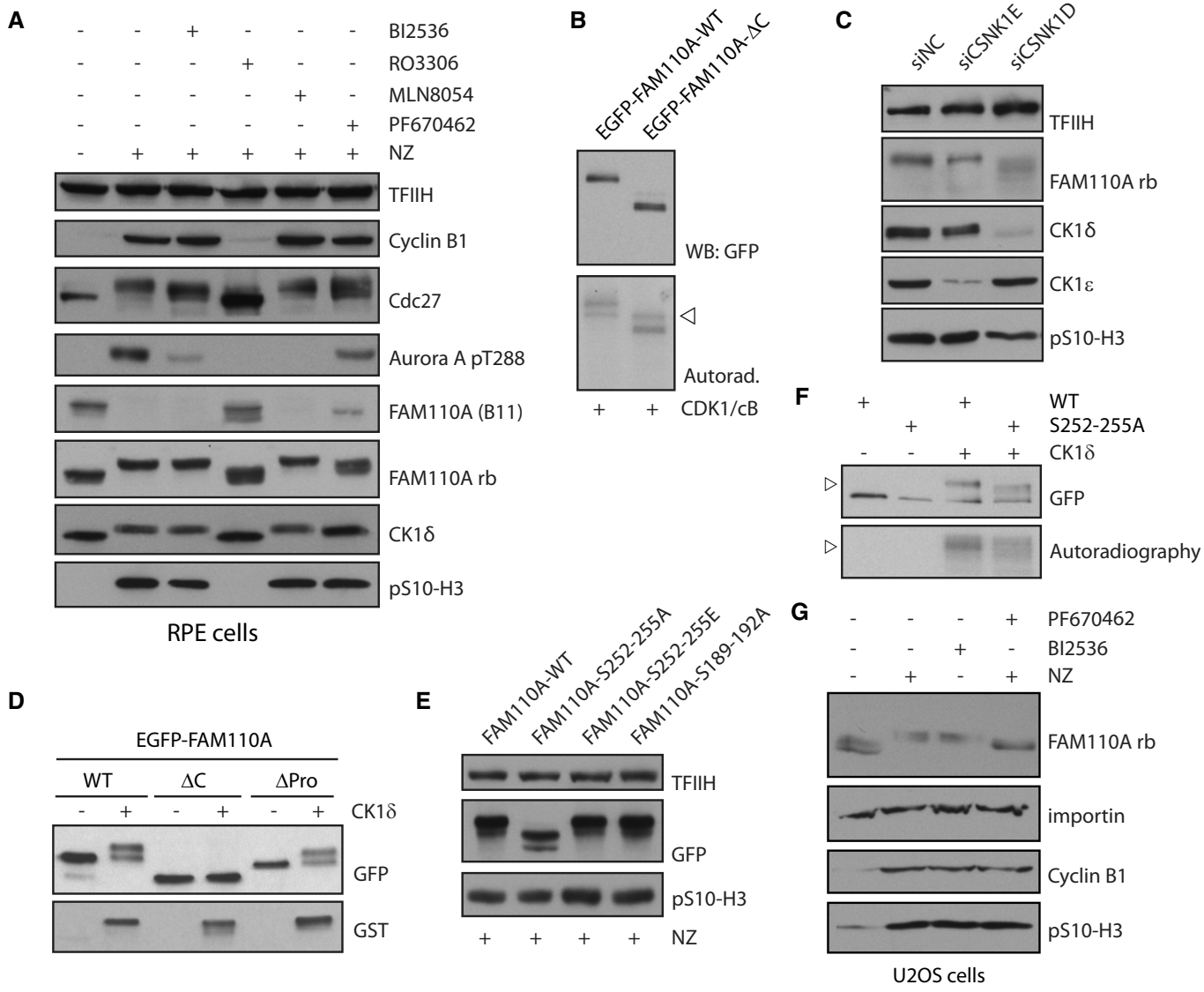

Figure 6. CK1 phosphorylates the C-terminal domain of FAM110A during mitosis.

A RPE cells arrested in mitosis by nocodazole (NZ) were treated with DMSO, PLK1 inhibitor BI2536 (100 nM), Aurora-A inhibitor MLN8054 (0.25 μM), CDK1 inhibitor RO3306 (20 nM), or CK1 inhibitor PF670462 (1 μM) for 60 min, collected, and analyzed by immunoblotting with indicated antibodies. Asynchronously growing RPE cells are shown for comparison (left line). Staining for H3-pS10 served as a marker of mitosis (n = 3).

B Isolated EGFP-FAM110A-WT or -ΔC proteins were incubated with active CDK1/GST-cyclin B1 in a kinase buffer containing ^{32}P-γATP for 20 min at 30°C. Phosphorylation was detected by autoradiography and position of FAM110A by immunoblotting. Empty arrowhead indicates position of CDK1.

C RPE cells were transfected with control, CSNK1D, or CSNK1E siRNA, and nocodazole was added 12 h before collecting the cells by mitotic shake-off. Whole-cell lysates were probed with indicated antibodies.

D EGFP-FAM110A-WT, -ΔPro, or -ΔC proteins isolated from transfected HEK293 cells using GFP-Trap were incubated with mock or with active GST-CK1δ for 20 min at 30°C. Mobility of the proteins was analyzed by immunoblotting (n = 2).

E Cells expressing the wild-type EGFP-FAM110A or its mutants were arrested in mitosis by nocodazole and collected by shake-off. Whole-cell lysates were analyzed by immunoblotting.

F Isolated EGFP-FAM110A-WT or -S252-255A proteins were incubated with mock or with active GST-CK1δ in the presence of ^{32}P-γATP for 30 min at 30°C. Phosphorylation of the substrate was detected by a mobility shift in immunoblotting with anti-GFP antibody or by autoradiography. Empty arrowhead indicates the same position on SDS–PAGE gel.

G U2OS cells were trapped in mitosis by overnight treatment with nocodazole or PLK1 inhibitor BI2536 (100 nM) and collected by mitotic shake-off. Part of the nocodazole-arrested cells was further treated with CK1 inhibitor PF670462 (1 μM) for 60 min. Whole-cell lysates were probed with indicated antibodies. Staining for pS10-H3 served as a marker of mitosis.

Source data are available online for this figure.

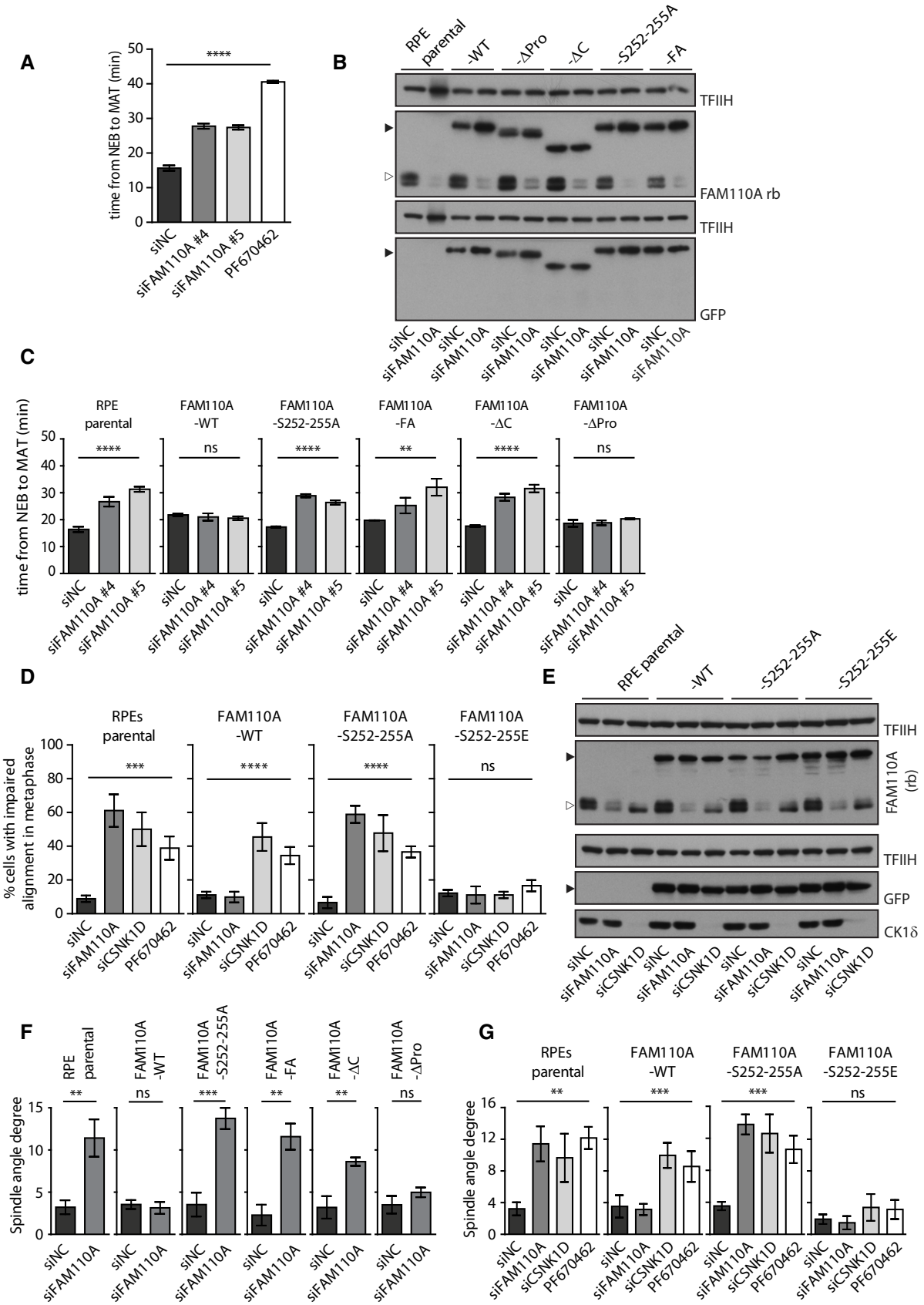
A
time from NEB to MAT (min)
siNC
siFAM110A #4
siFAM110A #5
PF670462
B
RPE parental
-WT
-ΔPro
-ΔC
-S252-255A
-FA
TFIIH
FAM110A rb
GFP
C
RPE parental
FAM110A -WT
FAM110A -S252-255A
FAM110A -FA
FAM110A -ΔC
FAM110A -ΔPro
D
RPEs parental
FAM110A -WT
FAM110A -S252-255A
FAM110A -S252-255E
% cells with impaired alignment in metaphase
siCSNK1D
E
-S252-255E
FAM110A (rb)
CK1δ
F
Spindle angle degree
G

Figure 7.

Figure 7. Mitotic function of FAM110A is controlled by its phosphorylation by CK1.

A U2OS-H2B-EGFP cells were transfected with indicated siRNAs for 48 h or were treated with PF670462 and filmed in 5-min intervals for 24 h. Time from nuclear envelope breakdown to MAT was quantified in 100 cells. Shown is mean of the medians ± SD ($n = 3$). Statistical significance was determined by ANOVA (****$P < 0.0001$).

B RPE cells or RPE cells stably expressing indicated EGFP-FAM110A variants were transfected with control (siNC) or FMA110A siRNA. Full arrow indicates migration of the EGFP-FAM110A-WT and empty arrow of endogenous FAM110A. Staining for TFIIH was used as a loading control.

C RPE cells or RPE cells stably expressing the wild-type or mutant EGFP-FAM110A were transfected with control or two various FAM110A siRNAs and were analyzed by time-lapse microscopy. Plotted are means of the medians of the time from NEB to MAT ± SDs. A hundred cells were quantified per condition ($n = 3$). Statistical significance was determined by ANOVA (****$P < 0.0001$ and **$P < 0.005$).

D RPE cells or RPE cells stably expressing indicated EGFP-FAM110A variants were transfected with control (siNC), FAM110A, or CSNK1D siRNA and grown for 48 h. Alternatively, cells were incubated with PF670462 for the last 12 h. Cells were treated with MG132 for 30 min prior fixation. Impaired chromosomal alignment was scored in > 30 metaphase cells per condition. Error bars indicate median ± SD. Statistical significance was determined by ANOVA ($n = 3$) (****$P < 0.0001$ and ***$P < 0.001$).

E Representative immunoblot analysis of samples from (D). Full arrow indicates migration of the EGFP-FAM110A-WT and empty arrow of endogenous FAM110A.

F RPE cells or RPE cells stably expressing indicated mutants were transfected with control or FAM110A siRNAs, fixed after 48 h, and stained for γ-tubulin. Metaphase cells were imaged by confocal microscopy (Z-stacks 0.5 μm), and spindle angle between the spindle axis and growth axis was determined. Plotted is a mean of medians from three repeats where 30 cells were imaged for each condition. Error bars indicate median ± SD. Statistical significance was determined ANOVA ($n = 3$) (***$P < 0.001$ and **$P < 0.005$).

G RPE cells or RPE cells stably expressing the wild-type FAM110A, −252-255A, or −252-255E mutants were transfected with control, FAM110A, or CSNK1D siRNAs. Alternatively, cells were treated with PF670462 (1 μM) for 12 h. Spindle angle was determined as in (F). Statistical significance was determined by ANOVA ($n = 3$) (***$P < 0.001$ and **$P < 0.005$).

Source data are available online for this figure.

CSNK1E (Fig 8A and B). In addition, we observed that the wild-type FAM110A but not the FAM110A-ΔC mutant localized to the mitotic spindle (Fig 8C and D). In addition, EGFP-FAM110A-C fragment showed strong enrichment at spindle poles indicating that the C-terminal domain is sufficient to promote binding to microtubules (Fig 8C and D). In contrast, EGFP-FAM110A-FA mutant deficient in interaction with CK1 showed poor localization to the spindle microtubules. Importantly, we observed that the amount of EGFP-FAM110A-S252-S255A mutant at the spindle pole was significantly reduced, although the localization defect was not as prominent as in the EGFP-FAM110A-FA mutant (Fig 8C and D). In contrast, EGFP-FAM110A-S252-S255E mutant showed normal localization at spindle poles (Fig 8C and D). Further, we observed that treatment of cells with CK1 inhibitor PF670462 impaired the ability of the wild-type EGFP-FAM110A to properly localize to the spindle poles (Fig 8E and F). In contrast, PF670462 treatment did not affect localization of the EGFP-FAM110A-S252-S255E mutant (Fig 8E and F). Finally, we tested the impact of CK1-dependent modification of FAM110A on the interaction with tubulin using immunoprecipitation (Fig 8G). We found that inhibition of CK1 impaired the interaction between the wild-type FAM110A and tubulin, whereas the FAM110A-S252-255E mutant bound tubulin also in the presence of PF670462. Consistent with the observed localization defect, the FAM110A-S252-255A mutant failed to interact with tubulin. In summary, we conclude that CK1-dependent phosphorylation of the S252–S255 region is involved in binding of FAM110A to the mitotic spindle although additional phosphorylation sites might further promote its interaction with microtubules.

Discussion

Here, we performed a transcriptomic analysis of diploid human RPE-FUCCI cells present in various stages of the cell cycle. The cell sorting protocol allowed us to avoid using cell synchronization that inherently activates the stress response, and thus, we believe that this data set might be a valuable source of information on the cell cycle-dependent expression in human non-transformed cells. In

Figure 8. FAM110A phosphorylation promotes its interaction with microtubules of mitotic spindle.

A RPE1 were transfected with control siRNA or CSNK1D siRNA or were treated with PF670462 prior fixation. Cells were probed with rabbit polyclonal to FAM110A and mouse monoclonal to γ-tubulin. Representative images are shown, and scale bars indicate 10 μm.

B Quantification of (A). Plotted is median FAM110A intensity at spindle poles positive for γ-tubulin ± SD. Each dot represents a single spindle pole. Statistical significance was determined by ANOVA ($n = 3$) (****$P < 0.0001$).

C Cells expressing the wild-type or mutant EGFP-FAM110A were fixed and stained for γ-tubulin and α-tubulin and analyzed by confocal microscopy (z-stack 0.16 μm). Representative images of maximal projections of the metaphase cells are shown, and scale bars indicate 10 μm. Merged images show signal of DAPI, γ-tubulin, and EGFP. Insets show a single Z plane at the spindle pole.

D Quantification of (C). Plotted is median EGFP intensity at spindle poles positive for γ-tubulin ± SD. Each dot represents a single spindle pole. Statistical significance was determined by ANOVA ($n = 3$) (***$P < 0.001$).

E Cells expressing the wild-type FAM110A or FAM110A-S252-255E mutant were treated with DMSO or with PF670462 for 6 h and were stained and imaged as in (C).

F Quantification of (E). Plotted is median EGFP intensity at spindle poles positive for γ-tubulin ± SD. Each dot represents a single spindle pole. Statistical significance was determined by ANOVA ($n = 3$) (***$P < 0.001$ and *$P < 0.05$).

G HEK293 cells transfected with indicated constructs were treated or not with PF670462 for 6 h. Pull-down from cell extracts was performed using GFP–Trap, and binding of tubulin was determined by immunoblotting ($n = 2$).

Source data are available online for this figure.Source data are available online for this figure.

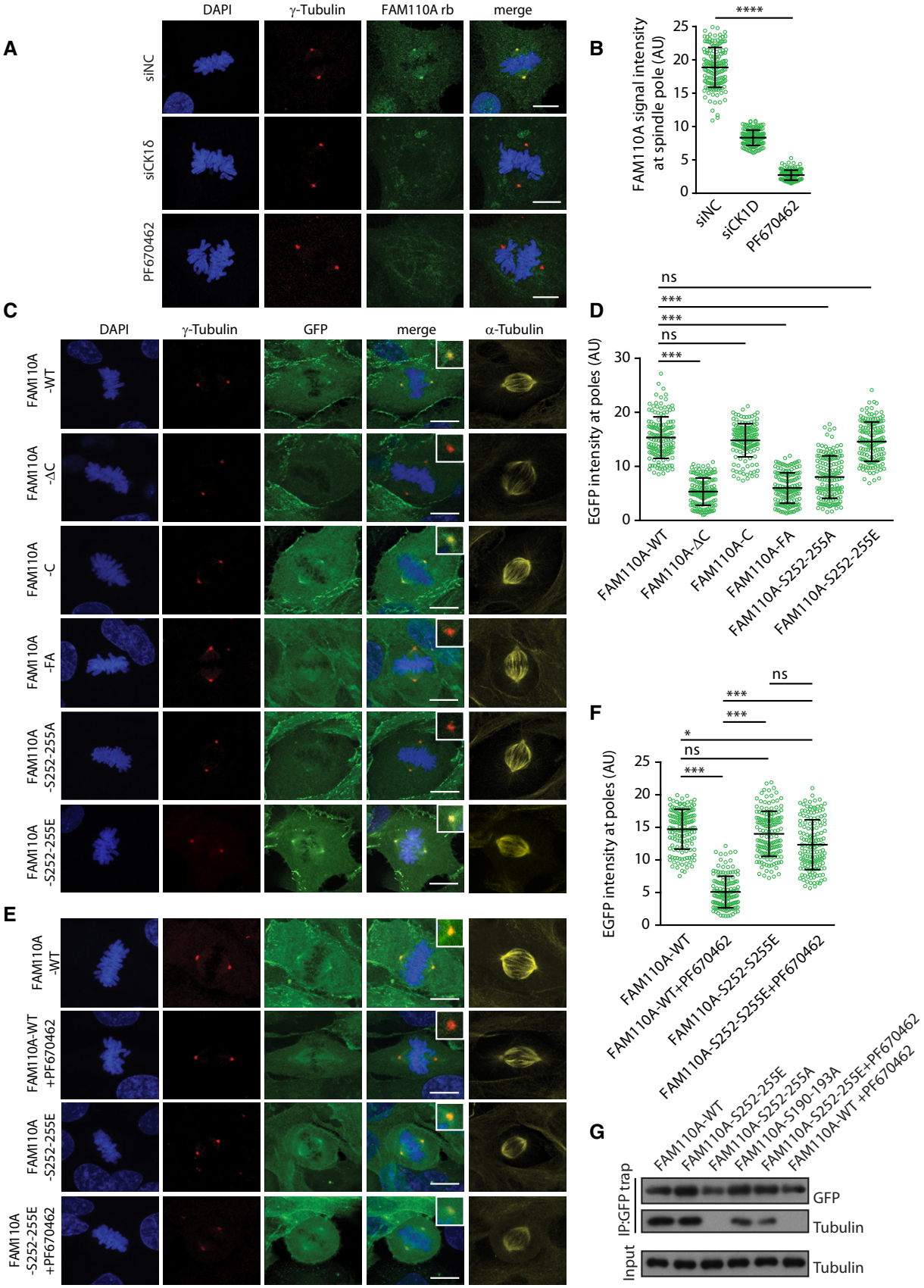

Figure 8.

total, we identified 701 differentially expressed transcripts between G1 and G2 cells and overall there is a good correlation with a recent study where various cell populations were sorted based on DNA staining (Van Rechem *et al,* 2020). As expected, we identified many genes with well-described function in the cell cycle control. In addition, we identified several genes, highly expressed in the G2 phase, the function of which still remains poorly understood. One of the strongest hits expressed in G2 cells was trophinin-associated protein TROAP (tastin) that has recently been shown to bind microtubules and to be required for bipolar spindle formation (NADANO *et al,* 2002; Yang *et al,* 2008). Helicase PIF1 is needed for DNA replication through G4 quadruplex structures and for maintenance of telomeric DNA (Mateyak & Zakian, 2006; Dewar & Lydall, 2010; Dahan *et al,* 2018). We observed strong enrichment of PIF1 mRNA in G2 cells but surprisingly not in the S phase cells. This suggests that other helicases than PIF1 might remove DNA quadruplexes during S phase, whereas PIF1 may take over in DNA replication of the late origins that occurs during G2. The E3 ubiquitin-protein ligase NEURL1B (also known as NEUR2) is involved in activation of Notch pathway during brain development in *Drosophila* but its function is poorly understood in vertebrates where it likely controls other processes than Notch signaling (Song *et al,* 2006; Taal *et al,* 2019). Here, we find that expression of NEURL1B is highly increased in G2 cells but its potential impact on the cell cycle progression remains to be determined. In G2 cells, we also observed strong expression of several genes with unknown function including family with sequence similarity 83 member D (FAM83D), family with sequence similarity 72 member D (FAM72D), and family with sequence similarity 110 member A (FAM110A). While this study was in progress, novel function of FAM83D in positioning of the mitotic spindle has been reported which is in good agreement with the observed expression profile (Fulcher *et al,* 2019).

Further, we followed with testing the role of previously uncharacterized protein FAM110A in mitosis. We found that FAM110A was diffusely distributed in the cytoplasm during interphase and was also present at the centrosome. During mitosis, FAM110A was enriched at spindle poles and proximal spindle microtubules where it colocalized with its previously reported interactor CSPP1 and with γ-tubulin. In telophase, FAM110A localized also to the cleavage furrow. Depletion of FAM110A with RNAi resulted in enrichment of the mitotic population and accumulation of cells exhibiting defects in the spindle organization and chromosomal alignment. This phenotype was rescued by expression of the mouse FAM110A confirming the specificity of the two independent siRNA oligonucleotides used in this study. Live cell imaging further revealed that FAM110A depletion slowed down progression through mitosis in particular by delaying the metaphase-to-anaphase transition. In addition, positioning of the mitotic spindle and orientation of the cell division was impaired in cells depleted of FAM110A.

Mobility shift observed in the SDS–PAGE suggested that FAM110A was massively post-translationally modified during mitosis. By combining small-molecule inhibitors and RNAi, we established that CDK1 and CK1 phosphorylate FAM110A during mitosis. Using *in vitro* kinase assay, we established that CDK1 phosphorylated the N-terminal domain of FAM110A, whereas CK1 phosphorylated the C-terminal tail. Subsequent site-directed mutagenesis identified S252-255 residues as substrates of CK1 although additional residues within the C-terminal domain might be also modified by CK1. Mass spectrometry and immunoprecipitation identified CK1 in complex with FAM110A, and this interaction was increased during mitosis compared to the interphase cells. Domain mapping revealed a short peptide sequence within the C-terminal domain of FAM110A mediating its interaction with CK1. Importantly, FAM110A-FA mutant deficient in CK1 binding as well as FAM110A-S252-255A mutant deficient in CK1 phosphorylation failed to rescue the loss of endogenous FAM110A in chromosomal alignment and progression through mitosis. In addition, we observed that inhibition of CK1 or depletion of CSNK1D by RNAi resulted in similar defect in positioning of the mitotic spindle. Interestingly, CSNK1A and its targeting to the spindle by interaction with FAM83D has recently been implicated in the spindle positioning (Fulcher *et al,* 2019). Our data suggest that other kinases of the conserved CK1 family also contribute to the control of the mitotic spindle organization. Importantly, we found that the phospho-mimicking FAM110A-S252-255E mutant rescued the chromosomal misalignment and spindle orientation defect upon depletion or inhibition of CSNK1D suggesting that FAM110A is a critical substrate of CSNK1D during mitosis. We propose that CSNK1D controls correct chromosomal alignment in metaphase through direct phosphorylation of the C-terminal tail of FAM110A that promotes its interaction with the mitotic spindle. As we observed displacement of LGN-GFP from the cell cortex in the proximity of misaligned chromosomes in FAM110A-depleted cells, we favor the possibility that the chromosomal aberrations contribute, at least in part, to the spindle positioning defect similarly as previously reported for depletion of CLIP-170 or CENP-E (Tame *et al,* 2016). Another striking possibility is that FAM110A could bridge spindle microtubules with actin cytoskeleton. Cortical actin cytoskeleton has been implicated in the spindle morphogenesis, and new roles for actin filaments directly at the mitotic spindle are emerging (Kunda *et al,* 2008; Mogessie & Schuh, 2017; Plessner *et al,* 2019). Using mass spectrometry and immunoprecipitation, we identified actin and tubulin as major interacting partners of mitotic FAM110A. The C-terminal domain of FAM110A was necessary and sufficient to bind to spindle microtubules, whereas it was disposable for interaction with actin suggesting that the interaction with actin and tubulin is mediated by distinct domains of FAM110A. Whether FAM110A regulates microtubule or actin dynamics during mitosis and to what extent this may contribute to control of the mitotic spindle orientation remains to be addressed by future research.

Materials and Methods

Antibodies and reagents

The following antibodies were used: mouse monoclonal antibodies against FAM110A (clones F4 and B11, Santa Cruz Biotechnology), rabbit polyclonal against FAM110A (Novus Biotechnology), rabbit polyclonal against γ-tubulin (Sigma Aldrich), mouse monoclonal against γ-tubulin (clone GTU-88, Sigma Aldrich), mouse monoclonal against α-tubulin (Biorbyt), CSNK1E (clone A-6), CSNK1D (clone C8), CSNK1A (clone H7) from Santa Cruz, CSPP1 (Proteintech), and beta-actin (clone D6A8, Cell Signaling). Small-molecule inhibitors BI2536, MLN8054, RO3306, and PF670462 were dissolved in DMSO and were from MedChemExpress.

Cells

Human hTERT-immortalized RPE1 cells (here referred to as RPE) were obtained from ATCC and were grown in DMEM supplemented with 6% FBS (Gibco), penicillin, and streptomycin. U2OS-tubulin-mCherry-H2B-Gfp were reported previously (Tanenbaum *et al,* 2008). Cells were regularly tested for mycoplasma infection using MycoAlert kit (Lonza). To generate RPE cells stably expressing the FUCCI indicator, we transfected RPE cells with pFucci-S/G2/M Green-Hyg plasmid, cultivated in media supplemented with hygromycin for 2 weeks, and selected cells expressing the reporter using Influx cell sorter (BD Biosciences) (Macurek *et al,* 2013). Subsequently, we transfected these cells with pFucci-G1 Orange plasmid, cultivated them for 2 weeks in media with geneticin, sorted single cells expressing the G1 reporter using Influx cell sorter (BD Biosciences), and expanded individual cell clones. The resulting RPE-FUCCI cells were tested for expression of both components of the FUCCI indicator by flow cytometry. RPE cells stably expressing EGFP-FAM110A were generated by transfection of linearized pEGFP-FAM110A plasmid followed by selection with geneticin for 3 weeks. Transfection of plasmid DNA was performed using Lipofectamine 2000 (Thermo Scientific) or by polyethylenimine. Transfection of Silencer Select siRNA oligonucleotides was performed using RNAiMAX (Thermo Scientific) at final concentration 5 nM. Targeting sequences are CAAUACAAGGUUUUUGACA for siRNA FAM110A#4, GGCUCCACCCUGUUGUGAA for siRNA FAM110A#5, and CCUGGGAAUGGAAAACUUU for siRNA FAM110B. Synchronization of cells at G1/S transition using a single thymidine block and subsequent release to mitosis was performed as described (Benada *et al,* 2015). Alternatively, cells arrested in mitosis by nocodazole were collected by shake-off, washed with PBS, and released to fresh media to allow exit from mitosis.

Plasmids

pFucci-S/G2/M Green-Hyg and pFucci-G1 Orange expressing hGeminin (1–110) and hCdt1 (30–120) fragments fused with fluorescent reporters were from MBL International (Sakaue-Sawano *et al,* 2008). pCMV6-FAM110A-Myc-DDK carrying the coding sequence for mouse FAM110A (NM_028666) was from OriGene. DNA fragment coding for FAM110A was subcloned into pEGFP-C1 backbone using Gibson assembly. Site-directed mutagenesis of the pEGFP-FAM110A was performed as described previously (Zheng *et al,* 2004). Numbering of the putative phosphorylation sites corresponds to sequence of the human FAM110A (NP_001035812). pEGFP-FAM110A-ΔC was generated by opening pEGFP-FAM110A with PstI and blunting with Klenow fragment. pEGFP-FAM110A-C was generated by ligation of the PstI/BamHI fragment of FAM110A (corresponding to amino acids 185–296) to pEGFP-C1. To generate pEGFP-FAM110A-N (corresponding to amino acids 1–136), the HindIII/BamHI fragment was removed from pEGFP-FAM110A, and the plasmid was blunted with Klenow and re-ligated. All constructs were validated by sequencing.

Cell sorting, RNA isolation, and BeadChip hybridization

Asynchronously growing RPE-FUCCI cells were collected by trypsinization, and RFP^+/GFP^- (corresponding to G1 cells) and RFP^-/GFP^+ (corresponding to G2 cells) populations (approx. 0.5×10^6 cells) were sorted using Influx cell sorter into RNAlater Stabilization Solution (Thermo Scientific). Total asynchronic population was collected as control. RNA was isolated by RNeasy Mini Kit (Qiagen), and its quality was verified by Qubit Fluorometer (Thermo Scientific). RNA was transcribed to cDNA by Illumina TotalPrep RNA Amplification Kit, hybridized to Illumina HumanHT-12_v4 Expression BeadChip, and scanned using BeadStation 500 (Illumina). Four biological replicates were processed in parallel on one BeadChip. Fold change in gene expression and statistical significance were calculated by limma software package (Ritchie *et al,* 2015).

Quantitative Real-Time Polymerase Chain Reaction (qRT–PCR)

RNA was isolated from RFP^+/GFP^- (corresponding to G1 cells), RFP^-/GFP^+ (corresponding to G2 cells), and RFP^+/GFP^+ (corresponding to S cells) RNeasy Mini Kit (Qiagen). cDNA was synthetized using 0.5 μg RNA, random hexamer, and RevertAid H Minus Reverse Transcriptase (Thermo Scientific). RT–qPCR was performed using LightCycler 480 SYBR Green I Master mix (Roche) using following cycle conditions: initial denaturation 95°C for 7 min, followed by 45 cycles of denaturation 95°C for 15 s, annealing 60°C for 15 s, and extension 72°C for 15 s. Ct values were determined using LightCycler 480 software. Data are presented as the ratio of the tested mRNA to *GAPDH* mRNA.

Cell synchronization

RPE cells were synchronized at G1/S transition by incubation in growth media supplemented with thymidine (2 mM) for 36 h. After two washes in PBS, cells were released to fresh medium and were collected at 2-h intervals. After 4 h from the release, nocodazole (100 ng/ml) was added to the media to arrest cells in prometaphase. All cells were collected by trypsinization, spinned down and lysed with Laemmli buffer or fixed with EtOH for FACS analysis. Alternatively, nocodazole-arrested cells were collected by mitotic shake-off at 16 h after release form thymidine block.

Flow cytometry (FACS)

Cells were fixed with 70% ice-cold EtOH, permeabilized by 0.5% Triton X-100 for 15 min at RT, and blocked with 1% BSA for 30 min. Subsequently, cells were incubated with pMPM-Cy5-conjugated antibody (Cell Signaling, 1:500) for 1 h at RT, washed with PBS, and re-suspended in PBS supplemented with DAPI (5 μg/ml). FACS analysis was performed using LSR II (BD Biosciences) and the FlowJo 10 software (Tree Star, BD). Single cells were gated using SSC and FSC, and mitotic cells were quantified using Cy5 channel.

Immunofluorescence

RPE cells grown on coverslips were fixed with 4% paraformaldehyde for 15 min at RT, washed with PBS, and permeabilized with 0.5% Triton X-100 for 10 min. Alternatively, cells were incubated with ice-cold methanol for 5 min. After washing with PBS, cells were blocked in 3% BSA for 30 min and incubated with primary antibodies for ours at RT. After washing with PBS, cells were incubated with Alexa Fluor-conjugated antibody for 1 h at RT. Coverslips were

subsequently washed 3 times in PBS, incubated with DAPI for 5 min at RT, and mounted on glass slides by VectaShield. Imaging was performed using Leica SP8 confocal microscope equipped with HC PL APO 63x/1.40 oil objective. Images were analyzed and processed using the LAS AF Lite software. For determining the mitotic spindle orientation, cells were grown on fibronectin-coated coverslips and were fixed 48 h after transfection with indicated siRNAs and stained for γ-tubulin. Metaphase cells were imaged by Leica SP8 confocal microscope at 0.5 μm z-stacks. Angle of the mitotic spindle relative to the growth surface was calculated from the linear distance between the spindle poles and the relative height distance of both spindle poles as described (Toyoshima & Nishida, 2007). For quantification of the wild-type or mutant EGFP-FAM110A at spindle poles, stable cell lines were fixed, stained for γ-tubulin and imaged by confocal microscopy. Mean pixel intensity of EGFP was determined in metaphase cells in a spherical region of interest determined by γ-tubulin signal. Similarly, endogenous FAM110A was stained with rabbit polyclonal FAM110A antibody and quantified at spindle poles in cells transfected by control siRNA, CSNK1D siRNA or treated by CK1 inhibitor. In total, 150 spindle poles were quantified in three independent experiments.

Time-lapse microscopy

U2OS-H2B-GFP/Tub-mCherry cells and parental RPE or RPE cells stably expressing EGFP-FAM110A variants were transfected with control or specific siRNA oligonucleotides and seeded into Lab-TekII coverglass chambers (Thermo Scientific). After 32 h post-transfection, subconfluent cells were imaged every 5 min for up to 24 h using Leica DMI6000 microscope equipped with N PLAN 40x/0.55 CORR DRY objective and with an 37°C, 5% CO_2 environmental chamber. Films were analyzed using LAS AF Lite software (Leica). Division kinetics was determined manually by counting each 5-min interval from the nuclear envelope breakdown to metaphase-to-anaphase transition. In total, 100 individual cells were quantified per condition in three independent experiments. To analyze orientation of the cell division, we measured the angle between the long axis determined in the interphase cell just before mitotic entry and the division axis determined in anaphase as described previously (He *et al,* 2017; Fulcher *et al,* 2019). Cells in which longitudinal axis was not apparent at G2/M transition were excluded from the analysis. Cell division was considered misoriented when the angle exceeded 15°. In total, 30 individual cells were quantified per condition in three independent experiments.

Immunoprecipitation and mass spectrometry

RPE cells stably expressing EGFP or EGFP-FAM110A were grown in the presence of nocodazole for 12 h, and mitotic cells were collected by shake-off and extracted in IP buffer (20 mM HEPES pH 7.5, 10% glycerol, 150 mM NaCl, 0.5% NP40) supplemented with cOmplete protease and PhosSTOP phosphatase inhibitors (Sigma) and sonicated for 3 × 20 s on ice. Cell extracts were centrifuged at 15,000 g for 10 min at 4°C and then incubated for 2 h with GFP-Trap beads (Chromotek). After three washes in IP buffer, bound proteins were eluted from beads by Laemmli buffer and analyzed by immunoblotting. Alternatively, bound proteins were analyzed by mass spectrometry using Orbitrap Fusion instrument (Thermo Scientific) and MaxQuant software. Three biological replicates were analyzed by mass spectrometry, and median peptide intensities were compared. Statistical significance was calculated using Student's *t*-test. Alternatively, cell extracts from EGFP-FAM110A cells were incubated with 2 μg of mouse IgG, CSNK1E or CSNK1D antibodies (all Santa Cruz) immobilized on Protein A/G UltraLink beads (Pierce) for 2 h and washed and bound proteins were analyzed by immunoblotting. Where indicated, cell extracts were prepared in RIPA buffer (25 mM Tris pH 7.6, 150 mM NaCl, 1.0% NP40, 1.0% sodium deoxycholate, and 0.1% SDS) to reduce background binding in immunoprecipitation.

In vitro phosphatase assay

Cells synchronized in G2 or in mitosis by overnight treatment with RO3306 or nocodazole, respectively, were extracted by RIPA buffer and spun down for 10 min at 4°C. Endogenous FAM110A was immunoprecipitated from cell extracts using rabbit polyclonal antibody (2 μg/reaction, Novus Biotechnologies) immobilized on pA/G beads. After washing four times in PBS, beads were incubated with mock or λ phosphatase (800 U/reaction, Santa Cruz) at 20°C for 30 min. Reaction was stopped by addition of 4× Laemmli buffer, and mobility of FAM110A was evaluated by immunoblotting.

In vitro kinase assay

Wild-type or mutant EGFP-FAM110A or EGFP alone was immunoprecipitated from transiently transfected HEK293 cells using GFP-Trap and the IP buffer supplemented by 1 M NaCl. Beads were washed three times in buffer containing high salt and then once in PBS and finally, bound proteins were eluted by 2 M glycine, immediately neutralized, and stored at −80°C. Purified proteins were checked by immunoblotting for the absence of co-purified protein kinases CDK1 and CK1. Purified proteins were incubated with 100 ng of GST-tagged CSNK1D (Sigma) in kinase buffer (10 mM HEPES pH 7.5, 2.5 mM β-glycerolphosphate, 1 mM EDTA, 4 mM $MgCl_2$, and 100 μM ATP) for 20 min at 30°C. Where indicated, kinase buffer was supplemented with 5 μCi of gamma-^{32}P-ATP. Reaction was stopped by mixing with 4× Laemmli buffer, and proteins were analyzed by immunoblotting.

Immunoblotting

Samples were separated by SDS–PAGE using 4–20% gels, transferred to nitrocellulose membrane, and probed with indicated primary and HRP-conjugated secondary antibodies, and signal was visualized using Peirce ECL substrate (Thermo Scientific). ImageJ software was used to quantify signal intensity in the rectangular regions of interest. After subtracting the background intensity, signal was normalized to the loading control from the identical blot. Three independent repeats were used for quantification.

Statistical analysis

Experiments were performed at least three times unless stated otherwise. Values in bar graphs are presented as mean ± SD. Statistical significance was evaluated using Student's two-tailed unpaired *t*-test or by ANOVA test in GraphPad Prism version 5.0 (GraphPad

Software), and P values ≤ 0.05 were considered significant ($^{*}P < 0.05$, $^{**}P < 0.005$, $^{***}P < 0.001$, and $^{****}P < 0.0001$).

Data availability

The complete data set from expression profiling of RPE-FUCCI cells was deposited in ArrayExpress database (https://www.ebi.ac.uk/arrayexpress/experiments/E-MTAB-9626/) under accession number E-MTAB-9626.

Expanded View for this article is available online.

Acknowledgements
We are thankful to Iain Cheeseman (Whitehead Institute for Biomedical Research) for providing HeLa-LGN-GFP cells, Pavel Talacko (OMICS facility, Charles University) for mass spectrometry analysis, Hynek Strnad (Genomics and Bioinformatics facility, IMG) for bioinformatic analysis, Ivan Novotny and Helena Chmelova (Light Microscopy Core Facility, IMG) for help with quantification of microscopic images, Vadym Sulimenko for sharing expertise with tubulin immunoprecipitation, and Zdenek Cimburek for cell sorting. This project was supported by Czech Science Foundation (17-04742S). Imaging was performed in Light Microscopy Core Facility supported by MEYS (LM2018129, CZ.02.1.01/0.0/0.0/18_046/0016045, Czech-BioImaging and LO1419) and OPPK (CZ.2.16/3.1.00/21547). Expression profiling was partially supported by RVO: 68378050-KAV-NPUI.

Conflict of interest
The authors declare that they have no conflict of interest.

Author contributions
CAP conducted most of the experiments and analyzed the data. MB and GJ performed the expression profiling. LM conceptualized and supervised the project, analyzed the data, and wrote the first draft of the manuscript. All authors edited the final version of the manuscript.

References

Badura L, Swanson T, Adamowicz W, Adams J, Cianfrogna J, Fisher K, Holland J, Kleiman R, Nelson F, Reynolds L *et al* (2007) An inhibitor of casein kinase Iε induces phase delays in circadian rhythms under free-running and entrained conditions. *J Pharmacol Exp Ther* 322: 730 – 738

Baldin V, Lukas J, Marcote MJ, Pagano M, Draetta G (1993) Cyclin D1 is a nuclear protein required for cell cycle progression in G1. *Genes Dev* 7: 812 – 821

Behrend L, Milne DM, Stöter M, Deppert W, Campbell LE, Meek DW, Knippschild U (2000) IC261, a specific inhibitor of the protein kinases casein kinase 1-delta and -epsilon, triggers the mitotic checkpoint and induces p53-dependent postmitotic effects. *Oncogene* 19: 5303 – 5313

Benada J, Burdová K, Lidak T, von Morgen P, Macurek L (2015) Polo-like kinase 1 inhibits DNA damage response during mitosis. *Cell Cycle* 14: 219 – 231

Bertoli C, Skotheim JM, de Bruin RAM (2013) Control of cell cycle transcription during G1 and S phases. *Nat Rev Mol Cell Biol* 14: 518 – 528

Bolderson E, Scorah J, Helleday T, Smythe C, Meuth M (2004) ATM is required for the cellular response to thymidine induced replication fork stress. *Hum Mol Genet* 13: 2937 – 2945

Brockman JL, Gross SD, Sussman MR, Anderson RA (1992) Cell cycle-dependent localization of casein kinase I to mitotic spindles. *Proc Natl Acad Sci USA* 89: 9454 – 9458

Chaudhry M, Chodosh L, McKenna G, Muschel R (2002) Gene expression profiling of HeLa cells in G1 or G2 phases. *Oncogene* 21: 1934 – 1942

Cheong JK, Hung NT, Wang H, Tan P, Voorhoeve PM, Lee SH, Virshup DM (2011) IC261 induces cell cycle arrest and apoptosis of human cancer cells via CK1δ/ε and Wnt/β-catenin independent inhibition of mitotic spindle formation. *Oncogene* 30: 2558 – 2569

Cho RJ, Campbell MJ, Winzeler EA, Steinmetz L, Conway A, Wodicka L, Wolfsberg TG, Gabrielian AE, Landsman D, Lockhart DJ *et al* (1998) A genome-wide transcriptional analysis of the mitotic cell cycle. *Mol Cell* 2: 65 – 73

Cooper S, Shedden K (2003) Microarray analysis of gene expression during the cell cycle. *Cell Chromosome* 2: 1

Cruciat C-M (2014) Casein kinase 1 and Wnt/β-catenin signaling. *Curr Opin Cell Biol* 31: 46 – 55

Dahan D, Tsirkas I, Dovrat D, Sparks MA, Singh SP, Galletto R, Aharoni A (2018) Pif1 is essential for efficient replisome progression through lagging strand G-quadruplex DNA secondary structures. *Nucleic Acids Res* 46: 11847 – 11857

Dewar JM, Lydall D (2010) Pif1- and Exo1-dependent nucleases coordinate checkpoint activation following telomere uncapping. *EMBO J* 29: 4020 – 4034

Fischer M, Grossmann P, Padi M, DeCaprio JA (2016) Integration of TP53, DREAM, MMB-FOXM1 and RB-E2F target gene analyses identifies cell cycle gene regulatory networks. *Nucleic Acids Res* 44: 6070 – 6086

Flotow H, Graves PR, Wang AQ, Fiol CJ, Roeske RW, Roach PJ (1990) Phosphate groups as substrate determinants for casein kinase I action. *J Biol Chem* 265: 14264 – 14269

Fulcher LJ, Bozatzi P, Tachie-Menson T, Wu KZL, Cummins TD, Bufton JC, Pinkas DM, Dunbar K, Shrestha S, Wood NT *et al* (2018) The DUF1669 domain of FAM83 family proteins anchor casein kinase 1 isoforms. *Sci Signal* 11: eaao2341

Fulcher LJ, He Z, Mei L, Macartney TJ, Wood NT, Prescott AR, Whigham AJ, Varghese J, Gourlay R, Ball G *et al* (2019) FAM83D directs protein kinase CK1α to the mitotic spindle for proper spindle positioning. *EMBO Rep* 20: e47495

Gallini S, Carminati M, De Mattia F, Pirovano L, Martini E, Oldani A, Asteriti IA, Guarguaglini G, Mapelli M (2016) NuMA phosphorylation by aurora-A orchestrates spindle orientation. *Curr Biol* 26: 458 – 469

Grant GD, Brooks L, Zhang X, Mahoney JM, Martyanov V, Wood TA, Sherlock G, Cheng C, Whitfield ML (2013) Identification of cell cycle–regulated genes periodically expressed in U2OS cells and their regulation by FOXM1 and E2F transcription factors. *Mol Biol Cell* 24: 3634 – 3650

Halicka D, Zhao H, Li J, Garcia J, Podhorecka M, Darzynkiewicz Z (2017) DNA damage response resulting from replication stress induced by synchronization of cells by inhibitors of DNA replication: analysis by flow cytometry. In *Cell Cycle Synchronization: Methods and Protocols*, Banfalvi G (ed), pp. 107 – 119. New York, NY: Springer New York

Hara M, Fukagawa T (2018) Kinetochore assembly and disassembly during mitotic entry and exit. *Curr Opin Cell Biol* 52: 73 – 81

Hauge H, Patzke S, Aasheim H-C (2007) Characterization of the FAM110 gene family. *Genomics* 90: 14 – 27

He Z, Kannan N, Nemirovsky O, Chen H, Connell M, Taylor B, Jiang J, Pilarski LM, Fleisch MC, Niederacher D *et al* (2017) BRCA1 controls the cell division axis and governs ploidy and phenotype in human mammary cells. *Oncotarget* 8: 32461 – 32475

van den Heuvel S, Dyson NJ (2008) Conserved functions of the pRB and E2F families. *Nat Rev Mol Cell Biol* 9: 713 – 724

Hornbeck PV, Zhang B, Murray B, Kornhauser JM, Latham V, Skrzypek E (2015) PhosphoSitePlus, 2014: mutations, PTMs and recalibrations. *Nucleic Acids Res* 43: D512 – 520

Isaacs RJ, Davies SL, Sandri MI, Redwood C, Wells NJ, Hickson ID (1998) Physiological regulation of eukaryotic topoisomerase II. *Biochim Biophys Acta* 1400: 121 – 137

Johnson Alyssa E, Chen J-S, Gould Kathleen L (2013) CK1 is required for a mitotic checkpoint that delays cytokinesis. *Curr Biol* 23: 1920 – 1926

Keenan CR, Langenbach SY, Jativa F, Harris T, Li M, Chen Q, Xia Y, Gao B, Schuliga MJ, Jaffar J *et al* (2018) Casein kinase 1δ/ε inhibitor, PF670462 attenuates the fibrogenic effects of transforming growth factor-β in pulmonary fibrosis. *Front Pharmacol* 9: 738

Kiyomitsu T, Cheeseman IM (2012) Chromosome- and spindle-pole-derived signals generate an intrinsic code for spindle position and orientation. *Nat Cell Biol* 14: 311 – 317

Knippschild U, Gocht A, Wolff S, Huber N, Löhler J, Stöter M (2005) The casein kinase 1 family: participation in multiple cellular processes in eukaryotes. *Cell Signal* 17: 675 – 689

Kotak S, Afshar K, Busso C, Gönczy P (2016) Aurora A kinase regulates proper spindle positioning in *C. elegans* and in human cells. *J Cell Sci* 129: 3015 – 3025

Kotak S, Busso C, Gönczy P (2013) NuMA phosphorylation by CDK1 couples mitotic progression with cortical dynein function. *EMBO J* 32: 2517 – 2529

Kraft C, Herzog F, Gieffers C, Mechtler K, Hagting A, Pines J, Peters JM (2003) Mitotic regulation of the human anaphase-promoting complex by phosphorylation. *EMBO J* 22: 6598 – 6609

Kunda P, Pelling AE, Liu T, Baum B (2008) Moesin controls cortical rigidity, cell rounding, and spindle morphogenesis during mitosis. *Curr Biol* 18: 91 – 101

Laoukili J, Alvarez M, Meijer LAT, Stahl M, Mohammed S, Kleij L, Heck AJR, Medema RH (2008) Activation of FoxM1 during G2 requires cyclin A/Cdk-dependent relief of autorepression by the FoxM1 N-terminal domain. *Mol Cell Biol* 28: 3076 – 3087

Laoukili J, Kooistra MRH, Brás A, Kauw J, Kerkhoven RM, Morrison A, Clevers H, Medema RH (2005) FoxM1 is required for execution of the mitotic programme and chromosome stability. *Nat Cell Biol* 7: 126 – 136

Lénárt P, Petronczki M, Steegmaier M, Di Fiore B, Lipp JJ, Hoffmann M, Rettig WJ, Kraut N, Peters JM (2007) The small-molecule inhibitor BI 2536 reveals novel insights into mitotic roles of polo-like kinase 1. *Curr Biol* 17: 304 – 315

Lindqvist A, Rodríguez-Bravo V, Medema RH (2009) The decision to enter mitosis: feedback and redundancy in the mitotic entry network. *J Cell Biol* 185: 193 – 202

Löhr K, Möritz C, Contente A, Dobbelstein M (2003) p21/CDKN1A mediates negative regulation of transcription by p53. *J Biol Chem* 278: 32507 – 32516

Ma HT, Poon RYC (2011) Synchronization of HeLa cells. In *Cell Cycle Synchronization: Methods and Protocols*, Banfalvi G (ed.), pp 151 – 161. Totowa, NJ: Humana Press

Macurek L, Benada J, Müllers E, Halim VA, Krejčíková K, Burdová K, Pecháčková S, Hodný Z, Lindqvist A, Medema RH *et al* (2013) Downregulation of Wip1 phosphatase modulates the cellular threshold of DNA damage signaling in mitosis. *Cell Cycle* 12: 251 – 262

Malumbres M, Barbacid M (2009) Cell cycle, CDKs and cancer: a changing paradigm. *Nat Rev Cancer* 9: 153 – 166

Manfredi MG, Ecsedy JA, Meetze KA, Balani SK, Burenkova O, Chen W, Galvin KM, Hoar KM, Huck JJ, LeRoy PJ *et al* (2007) Antitumor activity of MLN8054, an orally active small-molecule inhibitor of Aurora A kinase. *Proc Natl Acad Sci* 104: 4106 – 4111

Mateyak MK, Zakian VA (2006) Human PIF helicase is cell cycle regulated and associates with telomerase. *Cell Cycle* 5: 2796 – 2804

Milne DM, Looby P, Meek DW (2001) Catalytic activity of protein kinase CK1δ (Casein Kinase 1δ) is essential for its normal subcellular localization. *Exp Cell Res* 263: 43 – 54

Mogessie B, Schuh M (2017) Actin protects mammalian eggs against chromosome segregation errors. *Science* 357: eaal1647

Müller GA, Wintsche A, Stangner K, Prohaska SJ, Stadler PF, Engeland K (2014) The CHR site: definition and genome-wide identification of a cell cycle transcriptional element. *Nucleic Acids Res* 42: 10331 – 10350

Nadano D, Nakayama J, Matsuzawa S-I, Sato T-A, Matsuda T, Fukuda MN (2002) Human tastin, a proline-rich cytoplasmic protein, associates with the microtubular cytoskeleton. *Biochem J* 364: 669 – 677

Ohtsubo M, Theodoras AM, Schumacher J, Roberts JM, Pagano M (1995) Human cyclin E, a nuclear protein essential for the G1-to-S phase transition. *Mol Cell Biol* 15: 2612 – 2624

Okamura H, Garcia-Rodriguez C, Martinson H, Qin J, Virshup DM, Rao A (2004) A conserved docking motif for CK1 binding controls the nuclear localization of NFAT1. *Mol Cell Biol* 24: 4184 – 4195

Pagano M, Pepperkok R, Verde F, Ansorge W, Draetta G (1992) Cyclin A is required at two points in the human cell cycle. *EMBO J* 11: 961 – 971

Panbianco C, Weinkove D, Zanin E, Jones D, Divecha N, Gotta M, Ahringer J (2008) A casein kinase 1 and PAR proteins regulate asymmetry of a PIP(2) synthesis enzyme for asymmetric spindle positioning. *Dev Cell* 15: 198 – 208

Patzke S, Hauge H, Sioud M, Finne EF, Sivertsen EA, Delabie J, Stokke T, Aasheim H-C (2005) Identification of a novel centrosome/microtubule-associated coiled-coil protein involved in cell-cycle progression and spindle organization. *Oncogene* 24: 1159 – 1173

Peng Y, Moritz M, Han X, Giddings TH, Lyon A, Kollman J, Winey M, Yates J, Agard DA, Drubin DG *et al* (2015) Interaction of CK1δ with γTuSC ensures proper microtubule assembly and spindle positioning. *Mol Biol Cell* 26: 2505 – 2518

Pines J, Hunter T (1989) Isolation of a human cyclin cDNA: Evidence for cyclin mRNA and protein regulation in the cell cycle and for interaction with $p34^{cdc2}$. *Cell* 58: 833 – 846

Plessner M, Knerr J, Grosse R (2019) Centrosomal actin assembly is required for proper mitotic spindle formation and chromosome congression. *iScience* 15: 274 – 281

Portegijs V, Fielmich L-E, Galli M, Schmidt R, Muñoz J, van Mourik T, Akhmanova A, Heck AJR, Boxem M, van den Heuvel S (2016) Multisite phosphorylation of NuMA-related LIN-5 controls mitotic spindle positioning in *C. elegans*. *PLoS Genet* 12: e1006291

Ritchie ME, Phipson B, Wu D, Hu Y, Law CW, Shi W, Smyth GK (2015) limma powers differential expression analyses for RNA-sequencing and microarray studies. *Nucleic Acids Res* 43: e47

Rustici G, Mata J, Kivinen K, Lió P, Penkett CJ, Burns G, Hayles J, Brazma A, Nurse P, Bähler J (2004) Periodic gene expression program of the fission yeast cell cycle. *Nat Genet* 36: 809 – 817

Sadasivam S, Duan S, DeCaprio JA (2012) The MuvB complex sequentially recruits B-Myb and FoxM1 to promote mitotic gene expression. *Genes Dev* 26: 474 – 489

Sakaue-Sawano A, Kurokawa H, Morimura T, Hanyu A, Hama H, Osawa H, Kashiwagi S, Fukami K, Miyata T, Miyoshi H *et al* (2008) Visualizing spatiotemporal dynamics of multicellular cell-cycle progression. *Cell* 132: 487 – 498

Sakaue-Sawano A, Yo M, Komatsu N, Hiratsuka T, Kogure T, Hoshida T, Goshima N, Matsuda M, Miyoshi H, Miyawaki A (2017) Genetically encoded tools for optical dissection of the mammalian cell cycle. *Mol Cell* 68: 626 – 640

Sana S, Keshri R, Rajeevan A, Kapoor S, Kotak S (2018) Plk1 regulates spindle orientation by phosphorylating NuMA in human cells. *Life Sci Alliance* 1: e201800223

Santamaria A, Nagel S, Sillje HHW, Nigg EA (2008) The spindle protein CHICA mediates localization of the chromokinesin kid to the mitotic spindle. *Curr Biol* 18: 723 – 729

Sauer G, Körner R, Hanisch A, Ries A, Nigg EA, Silljé HHW (2005) Proteome analysis of the human mitotic spindle. *Mol Cell Proteomics* 4: 35

Saville MK, Watson RJ (1998) The cell-cycle regulated transcription factor B-Myb is phosphorylated by Cyclin A/Cdk2 at sites that enhance its transactivation properties. *Oncogene* 17: 2679 – 2689

Seldin L, Poulson ND, Foote HP, Lechler T (2013) NuMA localization, stability, and function in spindle orientation involve 4.1 and Cdk1 interactions. *Mol Biol Cell* 24: 3651 – 3662

Shedden K, Cooper S (2002) Analysis of cell-cycle-specific gene expression in human cells as determined by microarrays and double-thymidine block synchronization. *PNAS* 99: 4379 – 4384

Sillibourne JE, Milne DM, Takahashi M, Ono Y, Meek DW (2002) Centrosomal anchoring of the protein kinase CK1δ mediated by attachment to the large, coiled-coil scaffolding protein CG-NAP/AKAP450. *J Mol Biol* 322: 785 – 797

Song R, Koo B-K, Yoon K-J, Yoon M-J, Yoo K-W, Kim H-T, Oh H-J, Kim Y-Y, Han J-K, Kim C-H *et al* (2006) Neuralized-2 regulates a notch ligand in cooperation with mind bomb-1. *J Biol Chem* 281: 36391 – 36400

Srivastava S, Zasadzińska E, Foltz DR (2018) Posttranslational mechanisms controlling centromere function and assembly. *Curr Opin Cell Biol* 52: 126 – 135

Taal K, Tuvikene J, Rullinkov G, Piirsoo M, Sepp M, Neuman T, Tamme R, Timmusk T (2019) Neuralized family member NEURL1 is a ubiquitin ligase for the cGMP-specific phosphodiesterase 9A. *Sci Rep* 9: 7104

Takenaka K, Moriguchi T, Nishida E (1998) Activation of the protein kinase p38 in the spindle assembly checkpoint and mitotic arrest. *Science* 280: 599 – 602

Tame MA, Raaijmakers JA, Afanasyev P, Medema RH (2016) Chromosome misalignments induce spindle-positioning defects. *EMBO Rep* 17: 317 – 325

Tanenbaum ME, Macůrek L, Galjart N, Medema RH (2008) Dynein, Lis1 and CLIP-170 counteract Eg5-dependent centrosome separation during bipolar spindle assembly. *EMBO J* 27: 3235 – 3245

de Toledo S, Azzam E, Keng P, Laffrenier S, Little J (1998) Regulation by ionizing radiation of CDC2, cyclin A, cyclin B, thymidine kinase, topoisomerase IIalpha, and RAD51 expression in normal human diploid fibroblasts is dependent on p53/p21Waf1. *Cell Growth Differ* 9: 887 – 896

Toyoshima F, Nishida E (2007) Integrin-mediated adhesion orients the spindle parallel to the substratum in an EB1- and myosin X-dependent manner. *EMBO J* 26: 1487 – 1498

Uetake Y, Sluder G (2010) Prolonged prometaphase blocks daughter cell proliferation despite normal completion of mitosis. *Curr Biol* 20: 1666 – 1671

Van Rechem C, Ji F, Mishra S, Chakraborty D, Murphy SE, Dillingham ME, Sadreyev RI, Whetstine JR (2020) The lysine demethylase KDM4A controls the cell-cycle expression of replicative canonical histone genes. *Biochim Biophys Acta* 1863: 194624

Vigneron S, Sundermann L, Labbé J-C, Pintard L, Radulescu O, Castro A, Lorca T (2018) Cyclin A-cdk1-dependent phosphorylation of bora is the triggering factor promoting mitotic entry. *Dev Cell* 45: 637 – 650

Whitfield ML, Sherlock G, Saldanha AJ, Murray JI, Ball CA, Alexander KE, Matese JC, Perou CM, Hurt MM, Brown PO *et al* (2002) Identification of genes periodically expressed in the human cell cycle and their expression in tumors. *Mol Biol Cell* 13: 1977 – 2000

Yang S, Liu X, Yin Y, Fukuda MN, Zhou J (2008) Tastin is required for bipolar spindle assembly and centrosome integrity during mitosis. *FASEB J* 22: 1960 – 1972

Zheng L, Baumann U, Reymond JL (2004) An efficient one-step site-directed and site-saturation mutagenesis protocol. *Nucleic Acids Res* 32: e115